Report of Investigations 2017-8

UPDATED TSUNAMI INUNDATION MAPS FOR THE KODIAK AREA, ALASKA

E.N. Suleimani, D.J. Nicolsky, and R.D. Koehler

Published by
STATE OF ALASKA
DEPARTMENT OF NATURAL RESOURCES
DIVISION OF GEOLOGICAL & GEOPHYSICAL SURVEYS
2017

Cover Image. Damage from the 1964 Great Alaska Earthquake and tsunami. Image: National Oceanic and Atmospheric Administration (NOAA). http://www.photolib.noaa.gov/htmls/cgs02075.htm.

UPDATED TSUNAMI INUNDATION MAPS FOR THE KODIAK AREA, ALASKA

E.N. Suleimani, D.J. Nicolsky, and R.D. Koehler

Report of Investigations 2017-8

State of Alaska
Department of Natural Resources
Division of Geological & Geophysical Surveys

STATE OF ALASKA
Bill Walker, Governor

DEPARTMENT OF NATURAL RESOURCES
Andrew T. Mack, Commissioner

DIVISION OF GEOLOGICAL & GEOPHYSICAL SURVEYS
Steve Masterman, State Geologist and Director

Publications produced by the Division of Geological & Geophysical Surveys (DGGS) are available for free download from the DGGS website (dggs.alaska.gov). Publications on hard-copy or digital media can be examined or purchased in the Fairbanks office:

Alaska Division of Geological & Geophysical Surveys
3354 College Rd., Fairbanks, Alaska 99709-3707
Phone: (907) 451-5010 Fax (907) 451-5050
dggspubs@alaska.gov | dggs.alaska.gov

DGGS publications are also available at:
Alaska State Library,
Historical Collections & Talking Book Center
395 Whittier Street
Juneau, Alaska 99811

Alaska Resource Library and Information Services (ARLIS)
3150 C Street, Suite 100
Anchorage, Alaska 99503

Suggested citation:
Suleimani, E.N., Nicolsky, D.J., and Koehler, R.D., 2017, Updated tsunami inundation maps of the Kodiak area, Alaska: Alaska Division of Geological & Geophysical Surveys Report of Investigation 2017-8, 38 p., 10 sheets.
http://doi.org/10.14509/29740

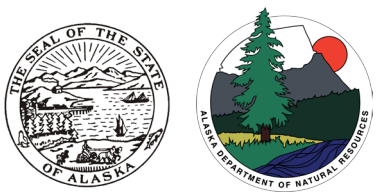

STATE OF ALASKA
Bill Walker, *Governor*

DEPARTMENT OF NATURAL RESOURCES
Andrew T. Mack, *Commissioner*

DIVISION OF GEOLOGICAL & GEOPHYSICAL SURVEYS
Steve Masterman, *State Geologist and Director*

Publications produced by the Division of Geological & Geophysical Surveys (DGGS) are available for download from the DGGS website (dggs.alaska.gov). Publications on hard-copy or digital media can be examined or purchased in the Fairbanks office:

Alaska Division of Geological & Geophysical Surveys
3354 College Rd., Fairbanks, Alaska 99709-3707
Phone: (907) 451-5010 Fax (907) 451-5050
dggspubs@alaska.gov
dggs.alaska.gov

CONTENTS

FIGURES

TABLES

APPENDIX

SHEETS

UPDATED TSUNAMI INUNDATION MAPS FOR THE KODIAK AREA, ALASKA

E.N. Suleimani[1], D.J. Nicolsky[1], and R.D. Koehler[2]

Abstract

The authors evaluated potential tsunami hazard for the communities of Kodiak, Womens Bay, and for the U.S. Coast Guard base on Kodiak Island by numerically modeling the extent of inundation from tsunami waves generated by hypothetical earthquake sources. Worst-case hypothetical scenarios are defined by analyzing results of a sensitivity study of the tsunami dynamics related to various slip distributions along the Alaska–Aleutian megathrust. The worst-case scenarios for the Kodiak communities are thought to be the subduction zone earthquakes offshore Kodiak Island with their greatest slip at 5–35 km (3.1–22 mi) depth. We also consider earthquakes as large as the 2011 Tohoku earthquake in Japan with the greatest slip located close to the trench area. The results show that the maximum predicted flow depth in downtown Kodiak could reach 13 m (42.6 ft), and the currents in Kodiak's Inner Harbor could be as strong as 3.7 m/sec (7.2 knots). The dangerous wave activity is expected to last for at least 10 hours after the earthquake. Results presented here are intended to provide guidance to local emergency management agencies in tsunami inundation assessment, evacuation planning, and public education to mitigate future tsunami hazards. This report updates the previously published assessment of tsunami hazard for the Kodiak Island communities.

INTRODUCTION

In Alaska, subduction of the Pacific plate under the North American plate has resulted in numerous great earthquakes and has the highest potential to generate tsunamis (Dunbar and Weaver, 2008). Several 20th century tsunamis generated during earthquakes along the Alaska–Aleutian subduction zone have resulted in widespread damage and loss of life in exposed coastal communities throughout the Pacific (Lander, 1996). However, tsunamis originating in the vicinity of the Alaska Peninsula, Aleutian Islands, and the Gulf of Alaska are considered a near-field hazard for Alaska, and could reach Alaska's coastal communities within minutes of an earthquake. Reducing property damage and loss of life is highly dependent on how well a community is prepared. Thus, estimating the potential flooding of the coastal zone in the event of a local or distant tsunami is an essential component of the preparedness process.

On March 27, 1964, the largest earthquake ever recorded in North America struck south-central Alaska. This M_w 9.2 megathrust earthquake (fig. 1) generated the most destructive tsunami in Alaska history and, farther south, impacted the west coast of the United States and Canada (Plafker and others, 1969; Kanamori, 1970; Johnson and others, 1996; Lander, 1996). Kodiak, the largest community on Kodiak Island, suffered great loss from the earthquake and the ensuing tsunami. Damage was primarily caused by 1.7 m (5.6 ft) of tectonic subsidence and a train of ten waves that inundated the low-elevation areas of the town (Kachadoorian and Plafker, 1967). In addition to the major tectonic tsunami, which was generated by an ocean-floor displacement between the trench and the coastline, more than 20 local tsunamis were generated by landslides in coastal Alaska during the 1964 earthquake (Lander, 1996). They arrived almost immediately after shaking was felt, leaving no time for warning or evacuation. Of the 131 fatalities associated with this earthquake, 122 were caused by tsunami waves (Lander, 1996).

This report updates the previously published report and tsunami hazard maps of the Kodiak area, Alaska (Suleimani and others, 2002). In the 15 years since the

[1]Geophysical Institute, University of Alaska, P.O. Box 757320, Fairbanks, Alaska 99775-7320; ensuleimani@alaska.edu
[2]Alaska Division of Geological & Geophysical Surveys, 3354 College Road, Fairbanks, Alaska 99709-3707; now at Nevada Bureau of Mines and Geology, Mackay School of Earth Science and Engineering, University of Nevada, Reno, 1664 North Virginia Street, MS 178, Reno, NV 89557

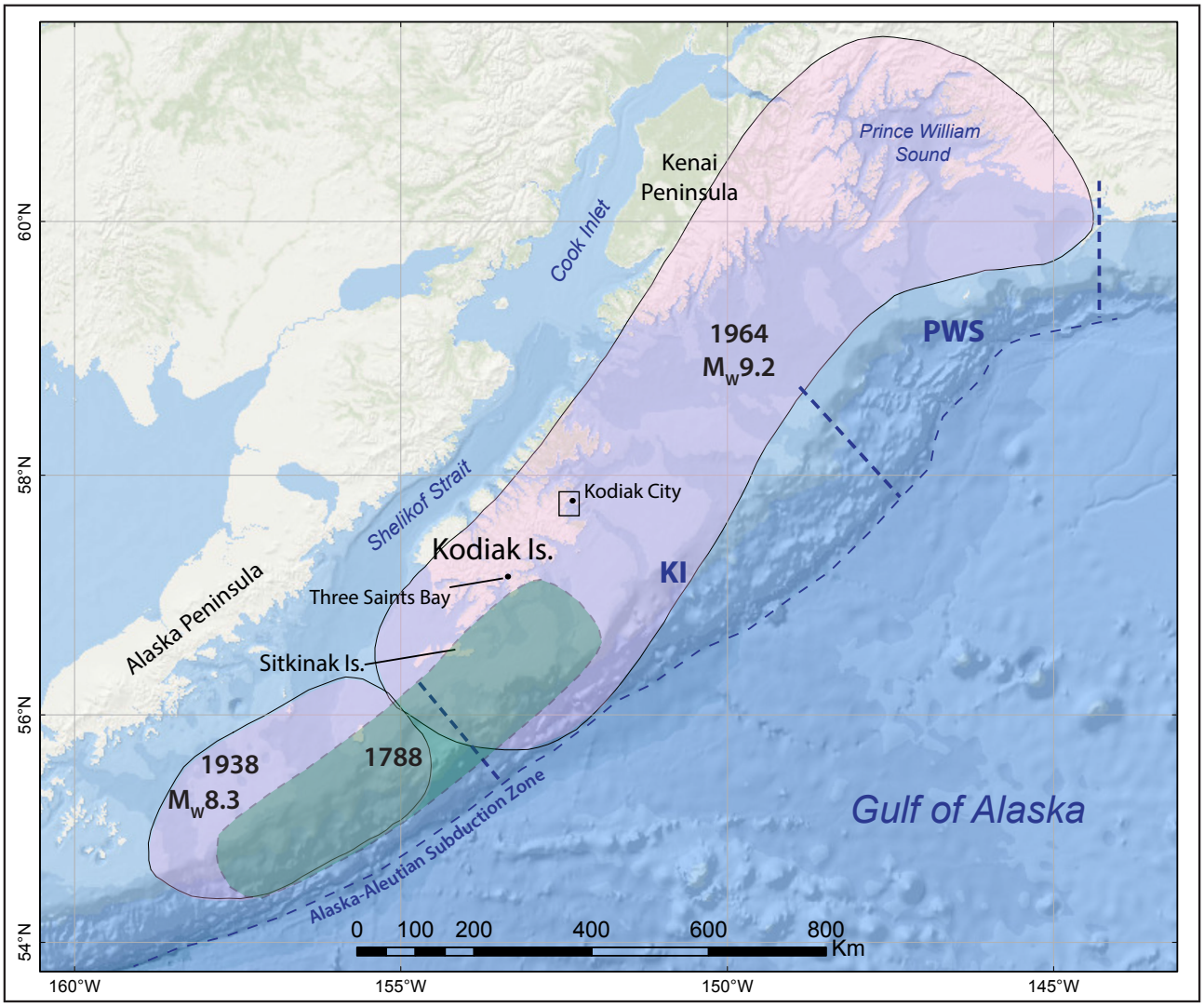

Figure 1. Map of south-central Alaska, showing the location of Kodiak Island and the rupture zones of the 1788, 1938, and 1964 Aleutian subduction zone earthquakes (shaded areas). The black rectangle marks the area shown in figure 2. KI = Kodiak Island asperity; PWS = Prince William Sound asperity.

publication of the original report, better bathymetric and topographic data for the Kodiak area became available. The tsunami disasters of 2004 in Indonesia and 2011 in Japan improved our understanding of the tsunami source mechanism, resulting in additional potential tsunami scenarios being included in our analysis of the Kodiak tsunami hazard. In this study we develop the worst-case credible tsunami scenarios for Kodiak coastal communities in support of long-term tsunami hazard mitigation activities.

The tsunami inundation maps for the Kodiak communities described in this report represent the results of the continuous combined effort of state and federal agencies to mitigate tsunami hazard in coastal Alaska. The intended audience of this report consists of scientists, engineers, and planners interested in the applied approach to develop tsunami inundation and evacuation maps. Digital data and documentation provided with the report enable technical users to explore the range of tsunami inundation possible for future events. The methodologies used to develop tsunami inundation maps are described in detail in multiple publications and are not reviewed in this report. Refer to Suleimani and others (2010, 2013, 2015, 2016) and Nicolsky and others (2011a, 2013, 2014, 2015) for a complete description of the process.

PROJECT BACKGROUND: REGIONAL AND HISTORICAL CONTEXT

SETTING

Kodiak is near the northwestern tip of Kodiak Island in the Gulf of Alaska at about 57°47'35" N, 152°23'39" W, approximately 405 km (252 mi) south of Anchorage and 2,298 km (1,428 mi) northwest of Seattle (figs. 1 and 2). Kodiak Island is the largest island in Alaska and is the second largest island in the United States. The following

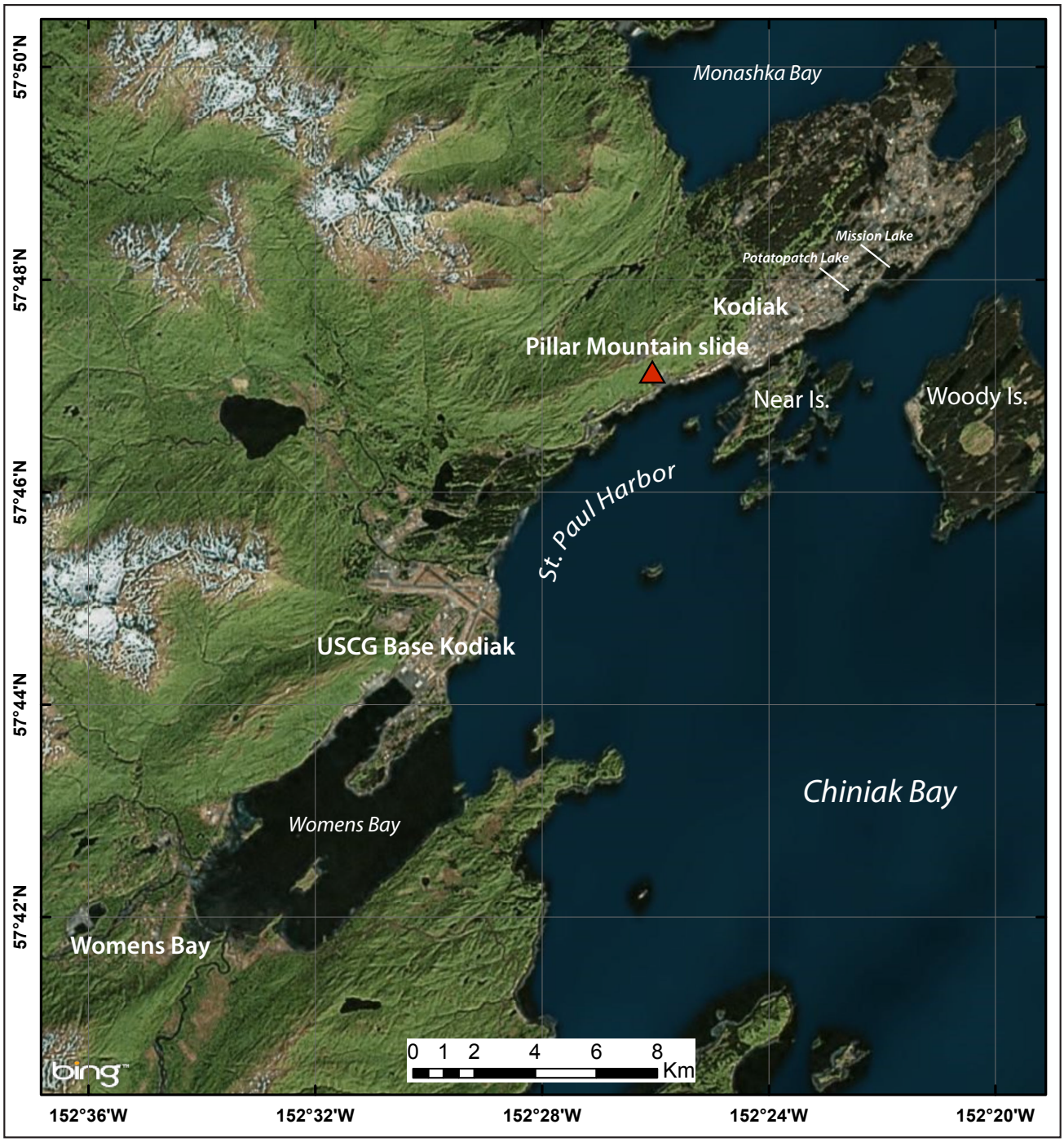

Figure 2. Map of Chiniak Bay and the Kodiak Island communities of Kodiak, U.S. Coast Guard Base Kodiak, and Womens Bay. The red triangle shows the location of the Pillar Mountain slide.

information is extracted from the Alaska Community Database maintained by the State of Alaska Division of Community and Regional Affairs of the Department of Commerce, Community, and Economic Development (DCCED/DCRA, 2015).

The island has been inhabited for the past 8,000 years. The first non-Native contacts were in 1763 by Russian Stephen Glotov and in 1792 by Alexander Baranov, a Russian fur trapper. Sea otter pelts were the primary incentive for Russian exploration, and a settlement was established at Chiniak Bay, the site of present-day Kodiak. At that time the island was called "Kikhtak", and later was known as "Kadiak", the Inuit word for island. In 1882 a fish cannery opened at the Karluk spit, sparking the development of commercial fishing in the area.

The Town of Kodiak was incorporated in 1940. During the Aleutian campaign of World War II, the U.S. Navy and the Army built bases on the island. Fort

Abercrombie was constructed in 1939 and later became the first secret radar installation in Alaska. Development continued, and the 1960s brought growth in commercial fisheries and fish processing. The 1964 earthquake and subsequent tsunami waves virtually leveled downtown Kodiak. The fishing fleet, processing plant, canneries, and 158 homes were destroyed, resulting in $30 million in damage. The infrastructure was rebuilt and, by 1968, Kodiak had become the largest fishing port in the U.S. in terms of dollar value. The local culture surrounds commercial and subsistence fishing activities. The U.S. Coast Guard comprises a significant portion of the community, and there is a large seasonal population. Kodiak is primarily non-Native, and the majority of the Native population is Alutiiq. A Russian Orthodox church seminary is based in Kodiak, one of only two existing Russian Orthodox seminaries in the United States. The Kodiak College, a branch of the University of Alaska Anchorage, is located in the city of Kodiak.

Kodiak Station is a U.S. Coast Guard Base, and is south of and adjacent to the city of Kodiak (fig. 2). This large tract of military property on Kodiak Island has been occupied since the Aleutian campaign of the WWII. Originally a U.S. Army base, it has also been a Naval base and is presently a Coast Guard base. The Air Force has also been active on Kodiak—they built a tracking station at Chiniak after the war. Kodiak Station houses about 1,500 military members and their families. The base is self-contained, providing its own water and sewer systems; however, many Coast Guard families live off base in the surrounding area.

The community of Womens Bay is 8 miles south of Kodiak (fig. 2), at the foot of Old Womens Mountain, along a bay of the same name. The Russian explorer Sarichev explored and named Womens Bay in the late 1700s. The area was extensively used during World War II by the military for national defense. The military placed infrastructure, particularly roads, in the area, some of which still exists. In the late 1960s the federal government transferred land to the State of Alaska. Some of this land, including the area presently occupied by the Womens Bay community, was subsequently transferred to the Kodiak Island Borough. Because of Womens Bay's close proximity to Kodiak Station, many of its residents are Coast Guard families. Approximately 12 percent of the population is Alaska Native.

SEISMIC AND TSUNAMI HISTORY

Kodiak Island is located at the eastern end of the Alaska–Aleutian subduction zone, the boundary along which the Pacific and North American plates converge (fig. 1). The rate of plate convergence near the island is approximately 60 mm (2.4 in) per year (DeMets and others, 1990). The eastern end of the megathrust has produced significant tsunamigenic earthquakes. On March 28, 1964, south-central Alaska was struck by the largest earthquake ever recorded in North America. This M_w 9.2 megathrust earthquake (fig. 1) generated a destructive tsunami that caused fatalities and great damage in Alaska, Hawaii, and the west coasts of the United States and Canada. The earthquake ruptured an 800-km-long (~500-mi-long) section of the Aleutian megathrust, producing vertical displacements over an area of about 285,000 km^2 (110,039 mi^2) in south-central Alaska (Plafker, 1969). The area of coseismic subsidence included Kodiak Island (KI), Kenai Peninsula, Cook Inlet, and part of northern Prince William Sound (PWS) (fig. 1). The major zone of uplift was seaward of the subsidence zone, in Prince William Sound and the Gulf of Alaska (Plafker, 1969). A number of communities on Kodiak Island suffered greatly from the resulting tsunami waves. The penultimate tsunami event in the area of Kodiak Island was recorded on July 21, 1788, when a strong earthquake near Sitkinak Island caused a 3-10 m tsunami that forced relocation of the first Russian settlement at Three Saints Bay on southwestern Kodiak Island (Lander, 1996) (fig. 1). Briggs and others (2014) present stratigraphic evidence of land level change and ^{137}Cs and ^{210}PB bracketing ages of a sand deposit that can be traced 1.5 km inland on Sitkinak Island (fig. 1) and suggest that the 1788 earthquake was a large megathrust rupture that generated the tsunami.

Analysis of historical earthquake data in the PWS and KI segments (Nishenko and Jacob, 1990) showed that the KI segment produced significant megathrust earthquakes more frequently and also independently of the PWS segment. Paleoseismic data also show that the KI segment ruptured independently in a large earthquake about 500 years ago—about 360 years more recently than the penultimate great earthquake that ruptured both the KI and PWS segments (Carver and Plafker, 2008). The PWS and KI segments have different recurrence intervals, with estimates of the recurrence interval for M_s 7.5–8 earthquakes in the KI segment being as low as 60 years (Nishenko, 1991).

Using seismic waveform data Christensen and Beck (1994) showed that there were two areas of high moment release during the 1964 Great Alaska Earthquake, representing the two major asperities of the 1964 rupture zone: the Prince William Sound asperity with an average slip of 18 m (59 ft), and the Kodiak Island asperity with an average slip of 10 m (33 ft) (fig. 1). The results of joint inversion of tsunami and geodetic data from the 1964 earthquake (Johnson and others, 1996) also suggest two areas of high moment release. Subsequent studies have shown that the PWS asperity is on the Yakutat–North American megathrust whereas the KI asperity is on the Pacific–North American megathrust (Ferris and others, 2003; Eberhart-Phillips and others, 2006; Worthington and others, 2010, 2012; Gulick and others, 2013). The

most recent deformation model of the 1964 earthquake was introduced by Suito and Freymueller (2009). This model was developed as a 3-D viscoelastic model in combination with an afterslip model, using realistic geometry with a shallow-dipping elastic slab. The purpose of the study was to describe the postseismic deformation that followed the 1964 earthquake. Important modifications in the fault geometry resulted in a revision of the 1964 coseismic model. The authors used the inversion-based model by Johnson and others (1996) as a basis for their coseismic slip model, adjusting it to the new geometry and critically reinterpreting the coseismic data. One critical change was the extension of the Montague Island high-angle splay fault from its subaerial outcrop to a longer length along the southern Kenai Peninsula coast to explain the pattern of subsidence in this area. The authors preferred forward finite-element modeling for calculation of coseismic slip due to inconsistency and systematic errors in coseismic displacement data. At the same time, their resulting slip distribution resembles that derived from inversion models of Holdahl and Sauber (1994), Johnson and others (1996), and Ichinose and others (2007).

On the basis of all published paleoseismic data for the region, Carver and Plafker (2008) calculate that the median intervals between the past eight great earthquakes M_w>8 in the PWS segment of the eastern Aleutian seismic zone range from 333 to 875 years, with an average of 589 years. Shennan and others (2014a) analyzed new paleoseismic field data from three sites in the PWS segment and revised the recurrence intervals of great earthquakes in the PWS segment. Their results suggest that the intervals range from ~420 to ~610 years, with a mean of ~535 years, excluding the interval between the 1964 earthquake and the penultimate event, which is ~883 years.

Recently Shennan and others (2014b) presented new paleoseismological data from Kodiak Island, which suggest that the intervals between ruptures of the Kodiak segments are shorter than previously assumed, and that the KI segment ruptured more frequently than the PWS segment. The authors tested the hypothesis of the Kodiak single-segment ruptures of 1788 and of ca. A.D. 1440–1620, which both occurred between the multi-segment ruptures of the 1964 earthquake and the earthquake of ca. A.D. 1020–1150, when the PWS and KI segments ruptured together (Carver and Plafker, 2008; Shennan and others, 2014a). Shennan and others (2014b) also analyzed the patterns of uplift and subsidence for the three most recent events on the KI segment, the 1964, the 1788, and the ca. A.D. 1440–1620 earthquakes, and found that the location of the hinge line, or the contour of zero deformation, was different for all three events.

Briggs and others (2014) presented stratigraphic evidence of land-level change and tsunami inundation during prehistoric and historical earthquakes west of Kodiak Island. They reported mixed uplift and subsidence records for Sitkinak Island (fig. 1), which suggests that it is located above a nonpersistent boundary near the edge of the 1964 rupture. This island experienced either uplift or subsidence depending on where the ruptures stopped along strike.

According to the National Centers for Environmental Information/World Data Centers (NCEI/WDS) Global Historical Tsunami Database (in progress) and Lander (1996), the city of Kodiak, U.S. Coast Guard Base Kodiak, and Womens Bay were impacted by multiple tsunamis in the past. Table 1 summarizes all historically recorded tsunami events that were experienced by the Kodiak Island communities considered in this report.

LANDSLIDE-GENERATED TSUNAMI HAZARDS

Tsunamis caused by underwater and subaerial slope failures are a significant hazard in the fjords of coastal Alaska and other high-latitude fjord coastlines (Lee and others, 2006). Kulikov and others (1998) analyzed tsunami catalog data for the North Pacific coast and showed that this region has a long record of tsunami waves generated by submarine and subaerial landslides, avalanches, and rockfalls. For example, as a result of the 1964 earthquake, numerous local submarine and subaerial landslide tsunamis were generated in Alaska, which accounted for 76 percent of the tsunami fatalities (Lander, 1996). Long-duration ground shaking of the 1964 earthquake triggered numerous rockslides, rockfalls, rotational slumps, and debris avalanches on the slopes of Kodiak Island. Plafker and Kachadoorian (1966) documented and classified the observed landslides and provided a map of the distribution of the larger landslides and slope failures on Kodiak Island. The majority of ground failures were located along the southeastern shore of the island; however, none of the landslides occurred along the shores of Chiniak Bay, which is the study area in this report.

The only documented landslide event in the Chiniak Bay area was the Pillar Mountain slide that occurred in 1971 near the city of Kodiak (fig. 2). During this event, over the period of one month, about 459,000 m^3 (~600,000 yd^3) of material failed and covered the main highway between the city of Kodiak and the Coast Guard base (Kachadoorian and Slater, 1978; Schlotfeldt and others, 2014). This slide was not earthquake-induced and did not produce any waves in St. Paul Harbor (Schlotfeldt and others, 2014). The authors concluded that the 1971 failure was initiated by oversteepening of the slope as a result of quarrying activity. Additionally, groundwater was interpreted to be an important part of the slope failure mechanism from pore water pressure buildup, caused by a cold spell and ice blocking at the surface (Schlotfeldt and others, 2014).

One of the uncertainties in the landslide scenario development process is related to determination of po-

Table 1. Tsunami effects for Kodiak communities; data from the National Geophysical Data Center Global Historical Tsunami Database (in progress) and comments from Lander (1996).

Date	Magnitude (M_W)	Origin	Maximum water height (m)	Comments
KODIAK CITY				
09/05/1866	?	Alaska Peninsula	?	Dock demolished on Woody Island
08/14/1868	8.5	Chile	2.22	Rising water forced workers from beach
04/01/1946	8.6	Eastern Aleutian Islands	0.61	Visible waves
03/28/1964	9.2	Gulf of Alaska	6.89	9 deaths; $31.3 million damage; five blocks of the business district destroyed (more than 215 structures); all but one docking facility destroyed
02/04/1965	8.7	Rat Islands	0.08	
10/17/1966	8.1	Peru	0.05	
03/03/1985	8.0	Chile	0.03	
03/06/1988	7.8	Gulf of Alaska	0.04	
07/30/1995	8.0	Chile	0.05	
06/10/1996	7.9	Andreanof Islands	0.07	
06/23/2001	8.4	Peru	0.04	
12/26/2004	9.1	Indonesia	0.13	
02/27/2010	8.8	Chile	0.36	
03/11/2011	9.0	Japan	0.35	
04/01/2014	8.2	Chile	0.08	
09/16/2015	8.3	Chile	0.22	
U.S. COAST GUARD BASE KODIAK (NAVAL AIR STATION KODIAK)				
03/28/1964	9.2	Gulf of Alaska	7.62	$10.3 million damage; total destruction of cargo dock and heavy damage to roads and bridges
WOMENS BAY				
11/04/1952	9.0	Kamchatka	0.12	
03/09/1957	8.6	Aleutian Islands	0.09	
05/22/1960	9.5	Chile	0.70	
03/28/1964	9.2	Gulf of Alaska	6.10	
05/07/1986	8.0	Aleutian Islands	0.03	

tential landslide volume. Schlotfeldt and others (2014) argued that although the strong ground shaking in 1964 lasted for about 5 minutes, it did not trigger any rockfalls around town. Also, they noted that several M 6.0 and larger earthquakes have occurred in the area since 1971 (a total of 17 earthquakes, according to the USGS database at http://earthquake.usgs.gov) without triggering any activity at the Pillar Mountain site. Numerical analyses of the future potential movement of the slope showed that deep-seated global failure is highly unlikely for Pillar Mountain in this location (Schlotfeldt and others, 2014). The 1971 failure was not deep-seated, and it took almost a month to complete the periodic dumps of slide material down the slope. Thus, there are significant uncertainties in the volume of slide material that could hypothetically reach water and generate a tsunami. Therefore, in this report we do not model tsunamis generated by a hypothetical mass failure at the site of the Pillar Mountain slide.

METHODOLOGY AND DATA

GRID DEVELOPMENT AND DATA SOURCES

We employed a series of nested computational grids in the Kodiak area to generate a detailed map of potential tsunami inundation triggered by local and distant earthquakes. The coarsest grid, with 2-arc-minute (approximately 2 km [~1.2 mi]) resolution, spans the central and northern Pacific Ocean. We used three intermediate grids between the coarsest- and highest-resolution grids (table 2; fig. 3). The highest-resolution level 4 grid (shaded rectangle in fig. 3) for the Kodiak communities covers Chiniak Bay, St. Paul Harbor, Monashka Bay, and Womens Bay (fig. 2). The spatial resolution of the high-resolution grid, with about 15 × 16 m (49.2 × 52.4 ft) cell dimensions, satisfies National Oceanic and Atmospheric Administration (NOAA) minimum recommended requirements for computation of tsunami inundation (National Tsunami Hazard Mitigation Program [NTHMP], 2010).

To develop the high-resolution level 4 grid, bathy-

Table 2. Nested grids used to compute propagation of tsunami waves generated in the Pacific Ocean to the Kodiak Island communities. The high-resolution grid is used to compute inundation. Note that the grid resolution in meters is not uniform: the first dimension is the longitudinal grid resolution and the second is the latitudinal resolution. Measurements also vary across each grid and are given for a reference location near Kodiak City to illustrate relative grid fineness.

Grid name	Resolution		Longitudinal Boundaries	Latitudinal Boundaries
	arc-seconds	meters (near Kodiak)		
Level 0, Northern Pacific	120 × 120	≈ 2,015 × 3,700	120°00' E – 100°00' W	10°00' N – 65°00' N
Level 1, South-central Alaska	24 × 24	≈ 403 × 740	156°00' W – 145°00' W	55°00' N – 62°00' N
Level 2, Coarse resolution, Kodiak Island	8 × 8	≈ 135 × 247	155°38'36" W – 149°50'33" W	56°01'45" N – 59°02'06" N
Level 3, Fine resolution, Kodiak Island	8/3 × 8/3	≈ 45 × 82	153°38'48" W – 151°51'31" W	57°32'22" N – 58°04'09" N
Level 4, High resolution, Kodiak City	8/9 × 1/2	≈ 15 × 16	152°36'55" W – 152°11'05" W	57°38'17" N – 57°51'04" N

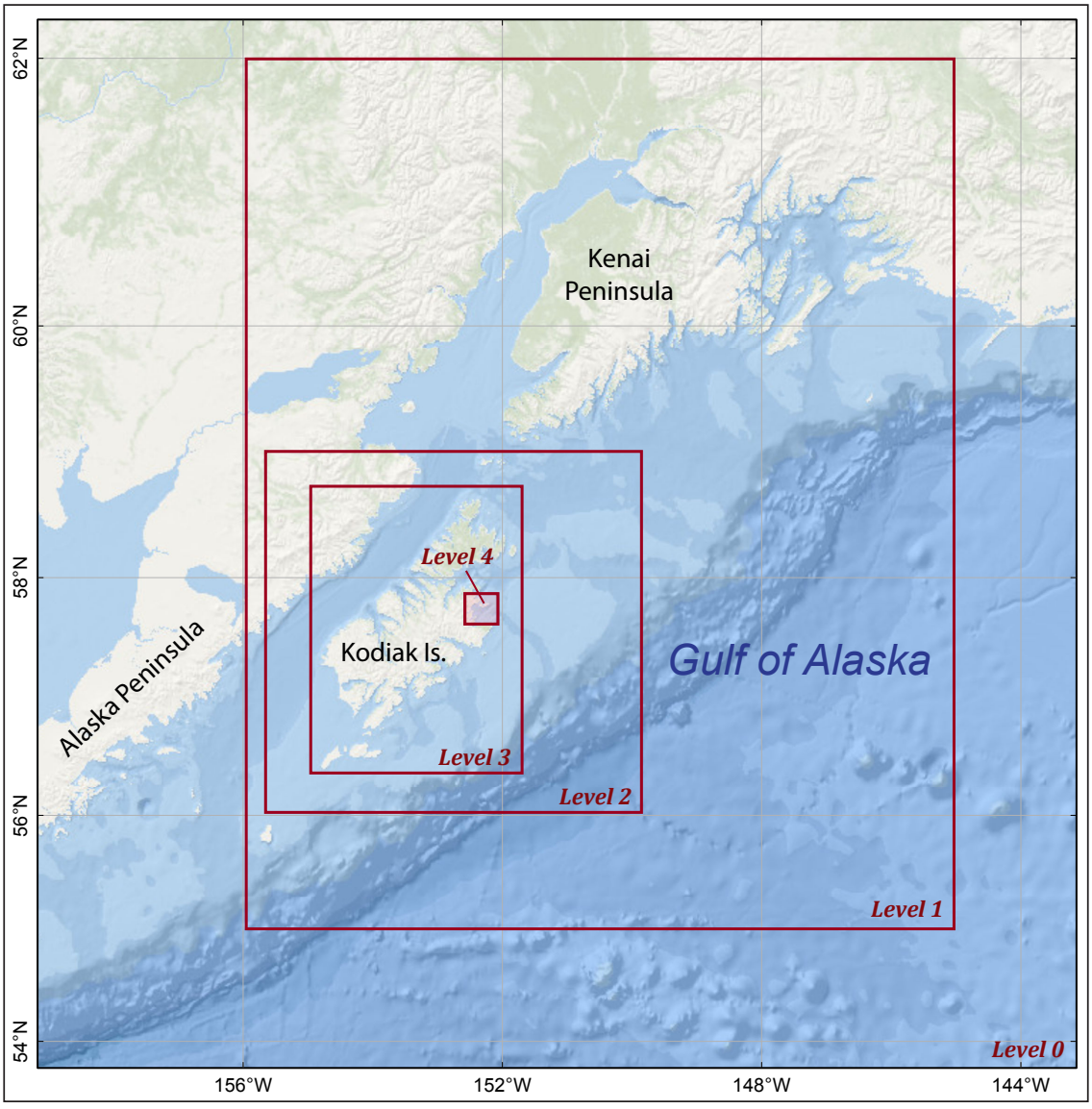

Figure 3. Nesting of the levels 0–4 bathymetry/topography grids for numerical modeling of tsunami propagation and runup in the Kodiak area. Each embedded grid is outlined by a red rectangle. The shaded rectangle for Level 4 corresponds to the area shown in figure 2.

metric, topographic, and shoreline digital datasets were obtained from various agencies, as described in Carignan and others (2013). The bathymetric datasets include National Ocean Service (NOS) hydrographic surveys, NOAA Electronic Navigational Chart (ENC) soundings, a U.S. Army Corps of Engineers (USACE) harbor survey, and multi-beam swath sonar surveys. The topographic datasets include the city of Kodiak bare-earth lidar DEM and the IFSAR DEM, the USGS NED (National Elevation Dataset) topographic DEM, and the USACE topographic points. More detailed information on grid development is contained in Lim and others (2009) and Carignan and others (2013).

NUMERICAL MODEL OF TSUNAMI PROPAGATION AND RUNUP

To estimate tsunami propagation and runup in the Kodiak area, we used the same numerical model employed in other Alaska tsunami inundation studies (for example, Suleimani and others, 2010, 2013, 2015, 2016, and Nicolsky and others, 2011a, 2013, 2014, 2015). All hypothetical tsunami simulations were conducted using the bathymetric/topographic data corresponding to the Mean Higher High Water (MHHW) tide level in the Kodiak communities. Since the employed numerical model of tsunami propagation and runup does not dynamically simulate interaction of tides and tsunami waves, we use a conservative approach and assume that the tsunami arrives at the communities on high tide.

VERIFICATION OF THE MODEL WITH THE MARCH 11, 2011, TOHOKU TSUNAMI

To test the accuracy of the grid nesting around the communities, we completed a model verification study of the Tohoku tsunami of March 11, 2011. We do not use observations of the 1964 tsunami in Kodiak to verify the numerical model, because it was shown by Suleimani, (2011) that results of near-field tsunami modeling are highly sensitive to the slip distribution in the rupture area. Since the observation sites on Kodiak Island are located within the rupture zone of the 1964 earthquake, even small variations in the slip pattern lead to sizable differences in modeling results. Also, the tide gauge at Kodiak was destroyed by the tsunami, and no other instrumental records exist for this area. We refer to Suleimani (2011) for detailed analysis of existing coseismic deformation models of the 1964 earthquake and results of the near-field modeling in Kodiak for the 1964 tsunami.

Using a method similar to that used by Nicolsky and others (2015), we compared modeling results with observed wave dynamics of the Tohoku tsunami at the Kodiak tide station on March 11 of 2011 (point 5 in fig. A1). We employed Shao and others' (2011) finite fault inversions model phase III, which predicts the vertical coseismic deformation shown in figure 4. The Tohoku tsunami produced a 0.38-m-high (1.25-ft-high) maximum wave in Kodiak (NCEI/WDS Global Historical Tsunami Database), whereas the simulation predicts a 0.42-m-high (1.38-ft-high) wave (fig. 5). Like Tang and others (2012), we observed an 11-minute time delay between the computed and observed waves. It was shown that systematic tsunami travel time delays (due to elasticity of the solid earth, seawater compressibility, and variations of gravitational potential) occur in many numerical experiments (Watada and others, 2014); a modeled tsunami may arrive up to 15 minutes sooner than the observed tsunami. The comparison between the computed and observed wave, adjusted for the arrival delay, shows that the simulated waveform reproduces well the phase of the first three recorded waves. The amplitudes of the first, second and third computed waves are about 15 percent, 40 percent, and 60 percent larger than the observed one, respectively. Bathymetric errors and uncertainty in the friction parameter might be contributing to the differences in amplitudes. The largest wave was observed about 18.5 hours after the earthquake and was probably caused by local effects. Overall, the model provides a conservative approximation to the recorded tsunami amplitudes in Kodiak, which indicates that the proposed coseismic deformation model adequately describes the coseismic slip distribution, and the DEM nesting is selected appropriately.

The far-field Tohoku tsunami did not result in a significant wave at Kodiak because of its distance from the tsunami source and directivity patterns of the energy propagation. However, other distant events might produce greater wave amplitudes in Kodiak and should not be dismissed without a proper evaluation.

TSUNAMI SOURCES

It is generally thought that all of the great historic earthquakes along the Alaska–Aleutian subduction zone occurred on the megathrust—the contact surface between the subducting Pacific plate and the North American plate. Because of friction the two converging plates generally cohere to each other and thus shear stress builds up between these plates along the megathrust. The shear stress is typically released instantaneously during an earthquake and the seismic energy propagates through the ground, causing strong shaking. It is theorized that the shear stress is primarily acquired in the locked or coupled regions of the megathrust, where the friction is greatest.

Zweck and Freymueller (2002) used a three-dimensional elastic dislocation model to demonstrate that the GPS data in southern Alaska can be satisfied by the presence of a locked area near southwest Prince William Sound and a locked area near southwest Kodiak Island. They found that locked areas correspond to the Prince

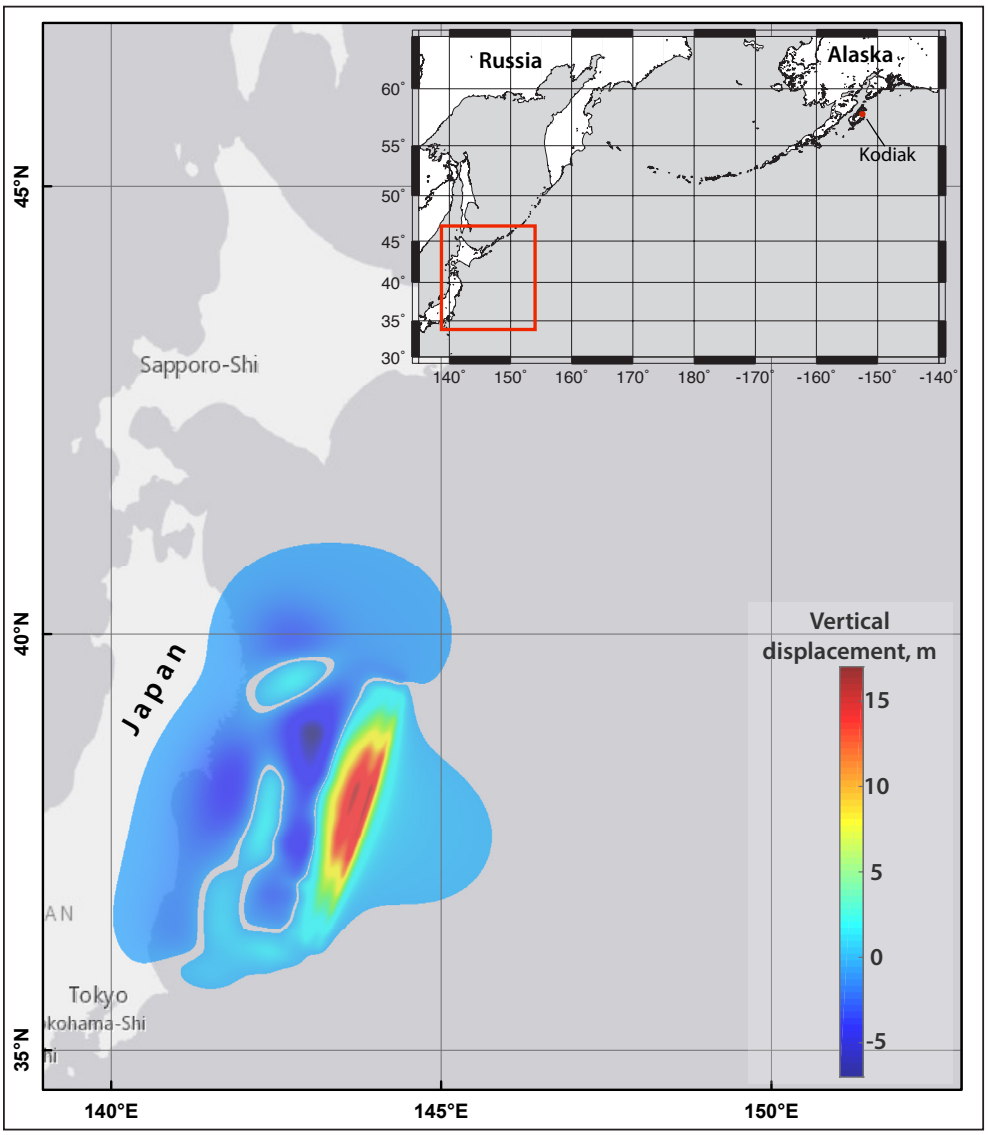

Figure 4. Map of vertical deformations of the ocean floor and adjacent coastal region corresponding to the March 11, 2011, Tohoku earthquake, based on a finite fault model by Shao and others (2011). Warm colors indicate uplift; blue indicates subsidence. Inset shows the location of the map with respect to the Kodiak tide gauge (red dot).

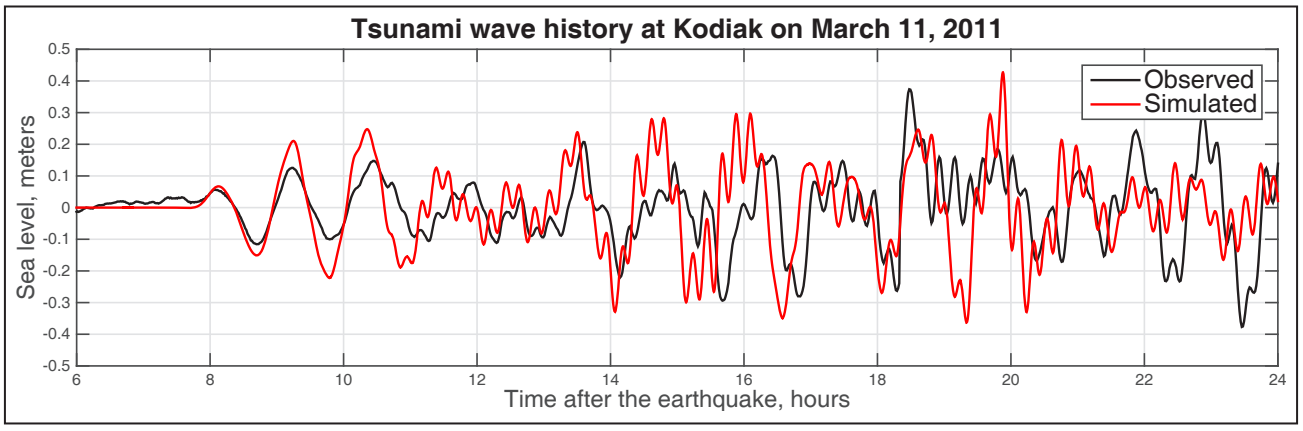

Figure 5. Observed and simulated water-level dynamics at the Kodiak tide station during the 24-hour period following the March 11, 2011, Tohoku earthquake.

William Sound and Kodiak Island asperities that ruptured in 1964, and that the locked regions repeat from one earthquake cycle to another. The authors showed that the site velocities on Kodiak Island are consistent with a model of locked elastic strain accumulation in the area of plate locking near Kodiak Island.

Recent paleoseismological findings indicate that prehistoric and historical earthquakes that occurred on the Kodiak segment of the Aleutian megathrust have different spatial patterns of coseismic deformation, in both the along-strike and downdip directions (Briggs and others, 2014; Shennan and others, 2014b). Locating the updip limit of the locked zone in the area of Kodiak Island is hindered by the lack of geodetic data close to the Aleutian trench, and this zone is essentially unconstrained by the land-based geodetic data. Seafloor GPS/acoustic measurements would be necessary to determine the existence or non-existence of high coupling at shallow depth. Recent studies comparing the Alaska and Tohoku margins (Kirby and others, 2013) propose that a hypothetical rupture might propagate to shallow depths, similar to that in the M_w 9.0 Tohoku earthquake, based on several similarities between the two margins. Therefore, to assess tsunami hazard for the Kodiak Island communities, we conducted a sensitivity study specific to the Kodiak area and investigated waves arriving from a variety of idealized ruptures placed at different downdip locations in the potentially locked region. The results of the sensitivity study were then applied to construct the maximum credible scenarios.

SENSITIVITY STUDY

The Kodiak Island area of the Aleutian megathrust is one of the two large segments of the 1964 rupture zone with a very wide locked region (200-250 km wide in the downdip direction), but the detailed shape of the locked region is uncertain (Freymueller and others, 2008). Therefore, we perform a sensitivity study to select slip distributions that maximize tsunami inundation for credible "worst-case" scenarios. In particular, we test the sensitivity of wave heights to coseismic slip originating at different downdip locations. Ruptures with slip at different depths result in different amounts of subsidence in coastal communities, and therefore in different effects due to incoming tsunami. We develop four hypothetical cases of the slip distribution (cases A–D) for M_w 8.0 earthquakes that could occur in the partially locked segment of the megathrust in the area of Kodiak Island (Freymueller and others, 2008) (fig. 6). The relative slip distribution for all four cases is identical: uniform in the along-strike direction with tapering at the ends of the rupture and a symmetrical bell-type slip curve in the downdip direction. Between any two consecutive cases, the hypothetical rupture is offset by about 10 km (6.2 mi) in the downdip direction: case A corresponds to a rupture at 40 km (25 mi) depth, case B corresponds to a rupture at 30 km (18.6 mi) depth, case C corresponds to a rupture at 20 km (12.4 mi) depth, and case D corresponds to a rupture at 10 km (6.2 mi) depth. The vertical deformation associated with each case is shown in figure 7. Blue shading indicates ground subsidence; red shading marks areas of uplift.

For each case, we calculate water dynamics near Kodiak and notice that simulated water levels in Kodiak vary considerably according to different slip distributions (fig. 8) The time series indicate that the rupture at 20 km (12.4 mi) depth (case C) results in the highest wave amplitude at all three locations. Case B, the rupture at 30 km (18.6 mi) depth, results in smaller wave amplitude, but with the earliest arrival. This means that if the rupture happens according to case B, the waves will start to arrive quickly—within 15 minutes of the earthquake. The deep rupture represented by case A produces a sizable coseismic uplift in the area of Chiniak Bay. As a result, the bay seabed and surrounding land surfaces become comparatively higher with respect to the post-earthquake sea level, and the arriving waves have much smaller amplitude. The wave generated from the shallow rupture of case D arrives later than the wave in case C, and also has smaller amplitude.

On the basis of the results of this downdip sensitivity study, we found that a rupture with the maximum slip placed at the depth of 20 km (12.4 mi) (case C) would likely have the most effect on tsunami height in Chiniak Bay. Therefore we developed hypothetical ruptures with maximum slip assigned to the 10–30 km (6.2–18.6 mi) depth range (related to cases B–D). We note that the considered cases represent hypothetical M_w 8.0 earthquakes, and that much larger earthquakes are possible in the Kodiak Island area (Carver and Plafker, 2008; Shennan and others, 2014b). As in Nicolsky and others (2016) we developed maximum credible scenarios for the Kodiak area communities by assuming a slip up to 35 m (115 ft) in the deep and intermediate sections of the Alaska–Aleutian megathrust and up to 55 m (180 ft) in the shallow sections of the megathrust. The maximum slip is assumed along regions of the megathrust that have the capability to generate the highest amplitude waves near Kodiak. We emphasize that the assumed slip distribution is consistent with earthquake source scenarios used by other tsunami modeling studies (for example, Butler, 2014; USGS SAFRR scenario, https://www2.usgs.gov/natural_hazards/safrr/projects/tsunamiscenario.asp).

CONSIDERED TSUNAMI SCENARIOS

In this section, we list scenarios describing tsunamigenic earthquakes in the Kodiak area. In the previously published tsunami hazard assessment report for Kodiak, Suleimani and others (2002) modeled a repeat of the 1964 Great Alaska Earthquake, some modifications of that

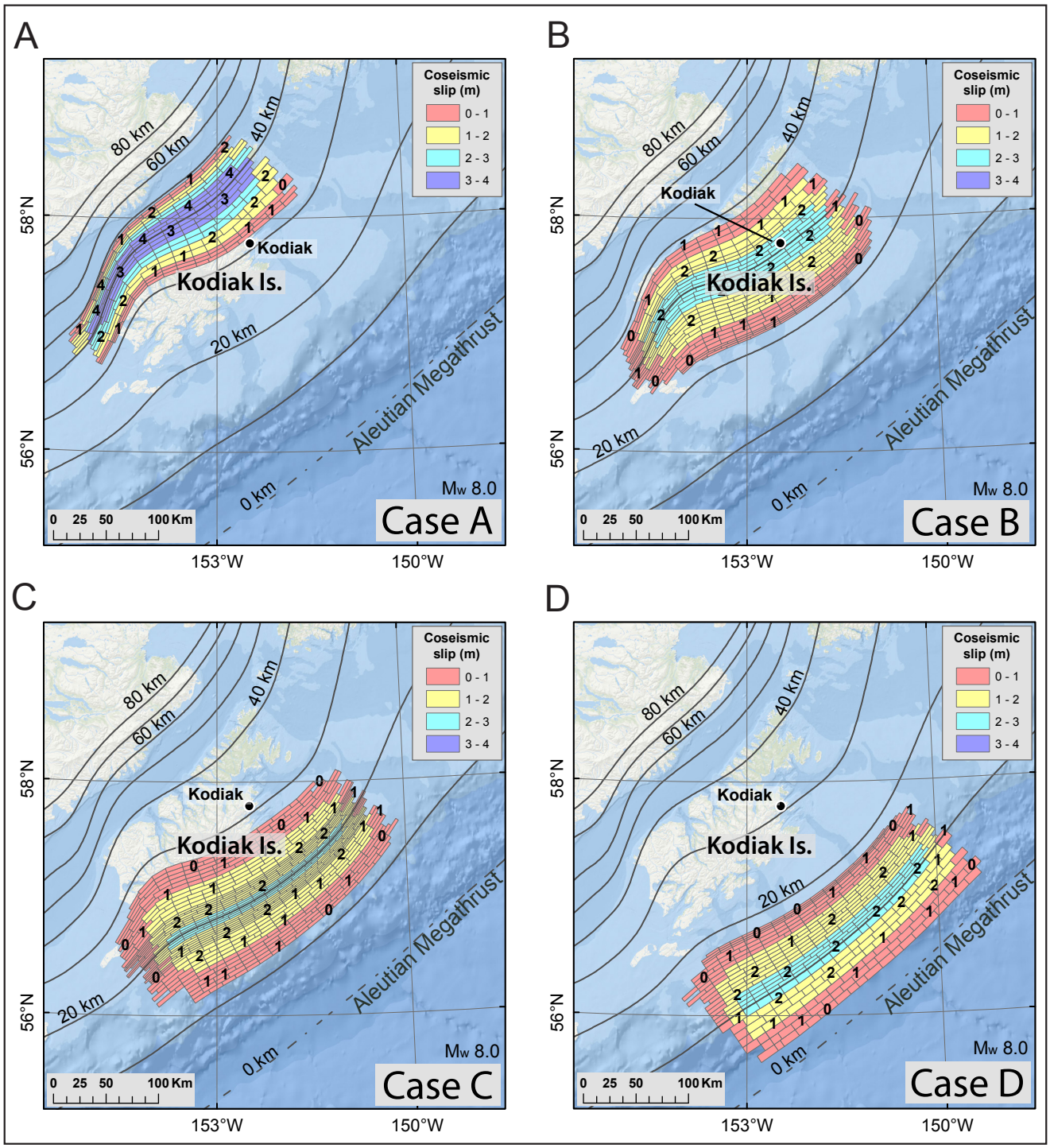

Figure 6. Hypothetical slip distributions along the plate interface for cases A–D, modeling M_w8.0 ruptures in the area of Kodiak Island. The slip location varies in the downdip direction of the plate interface while preserving the same patch configuration. Black numbers show the value of slip and heavy black lines are depth contours of the subduction interface, in meters.

earthquake, and a rupture of the Cascadia subduction zone. Similar to the Suleimani and others (2002) report, we also consider a scenario describing the repeat of the 1964 earthquake (scenario 1). However, other scenarios (in particular, scenarios 2-7) are now based on results of the sensitivity study and larger considered co-seismic slip. Previously, the co-seismic slip was limited to 14.5 m (47 ft) near the trench along Kodiak Island (Suleimani and others, 2002, Figure 4). Now, following modeling results by Kirby and others, (2013) from the USGS Science Application for Risk Reduction (SAFRR) project (Ross and others, 2013) and reconstructions of the co-seismic slip for the 2011 Tohoku earthquake by Shao and others (2011), we assume that the maximum slip near the trench could be up to 50 m (160 ft). Also, for the sake of consistency with previous reports (e.g., Nicolsky and others, 2016; Suleimani and others, 2016), we consider earthquakes (scenarios 8 and 9) with slip parameterization according to the research by Butler and others (2014). Scenario 10 models a rupture of the Cascadia subduction zone.

In all scenarios, we do not account for the finite speed of rupture propagation along the fault, and we consider the ocean-bottom displacements to be instantaneous. All examined scenarios are summarized in table 3.

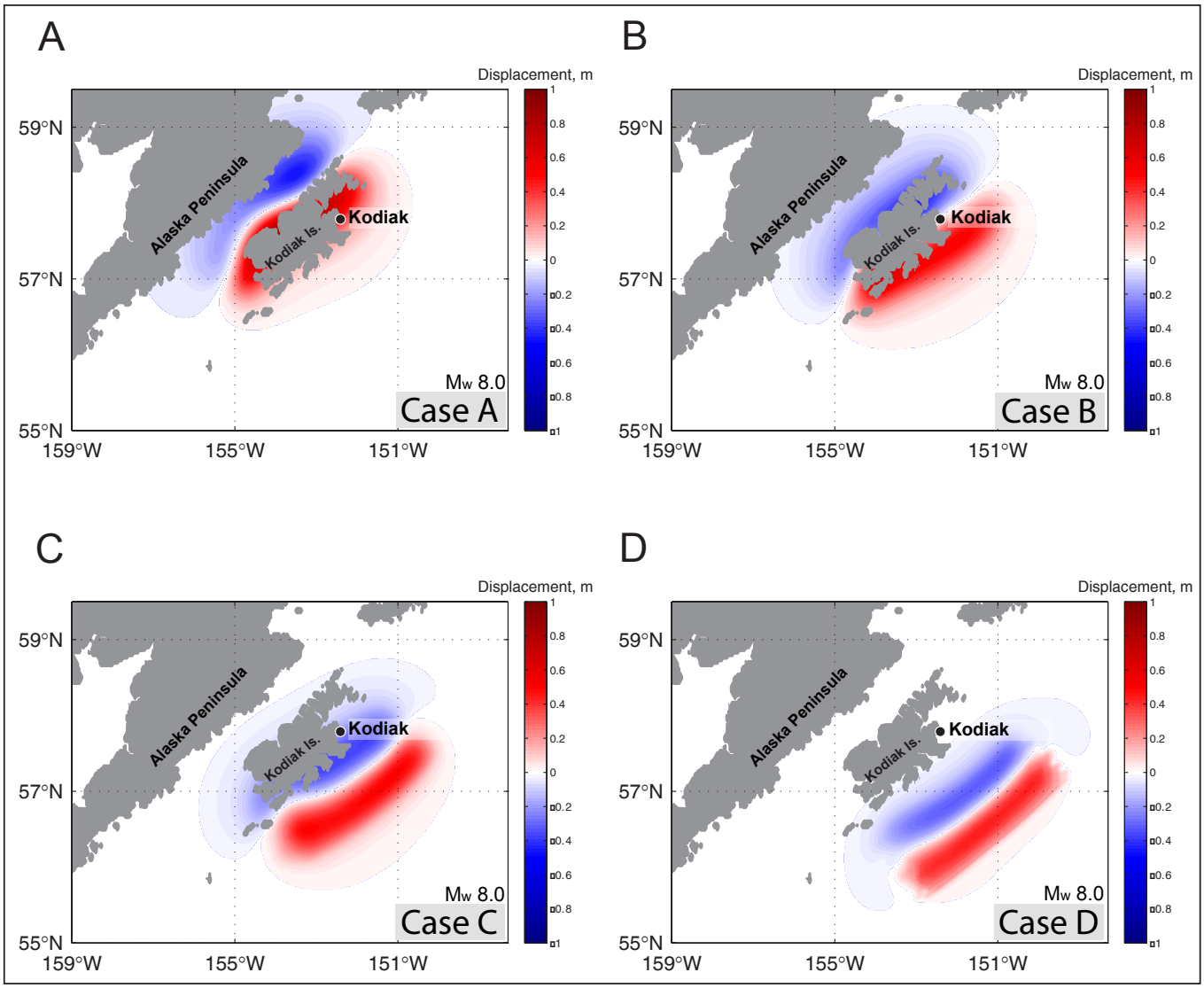

Figure 7. Computed vertical ground-surface deformation related to cases A–D shown in figure 6. Blue areas are associated with coseismic surface subsidence; areas of uplift are shown in red.

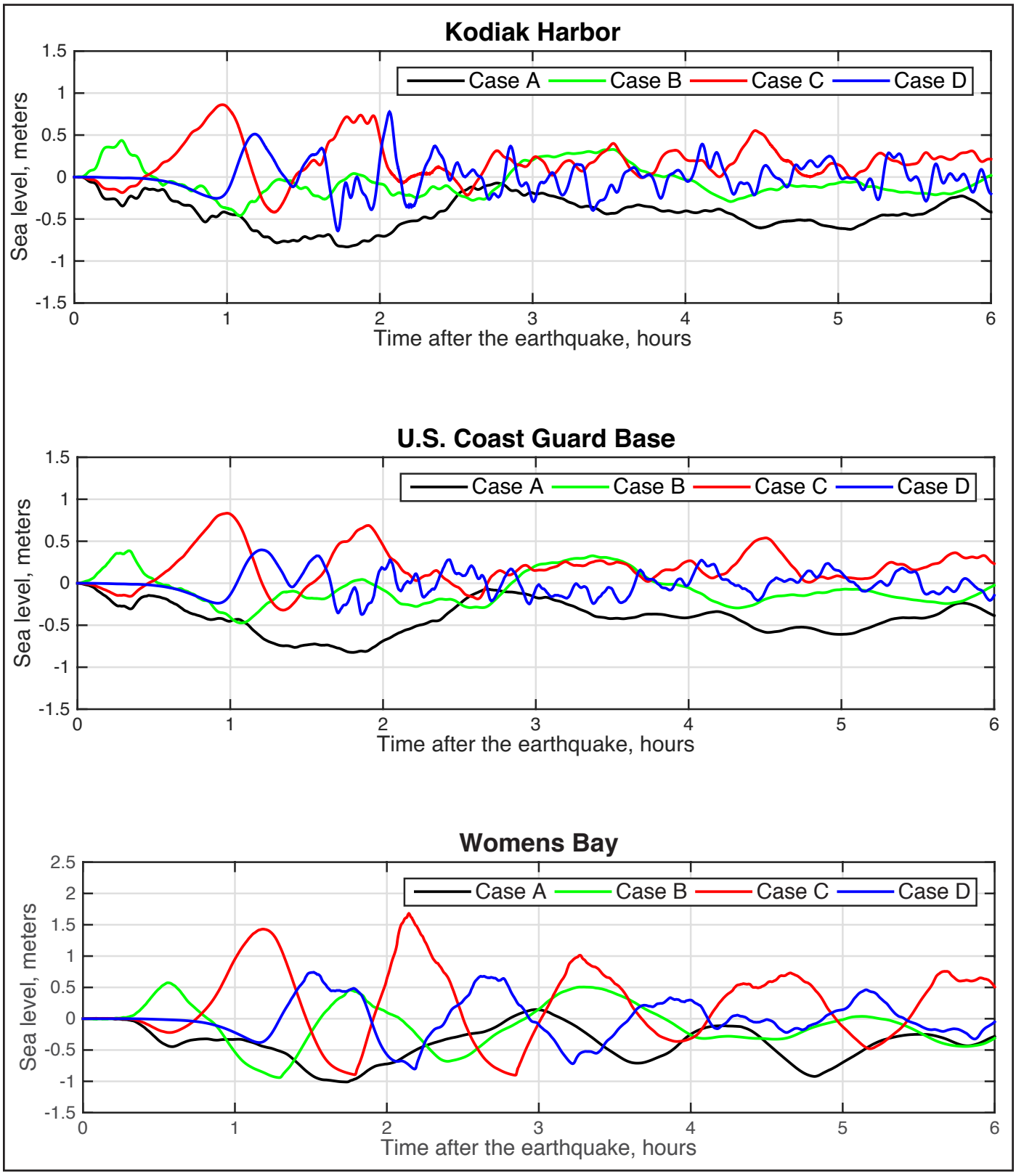

Figure 8. Modeled water-level dynamics at three locations in Chiniak Bay for the ground-surface deformations shown in figure 7.

Table 3. All hypothetical scenarios used to model tsunami runup in the Kodiak area. Scenario marked by an asterisk (*) indicates scenario 16 of the King Cove and Cold Bay modeling study by Suleimani and others (2016). Map Sheets 6-10 show potential permanent flooding in the Kodiak area due to coseismic subsidence.

Tectonic Scenarios		Depth range (km)	Depth range of maximum slip (km)	Maximum slip (m)	Maximum subsidence (m)	Maximum uplift (m)	Vertical displacement in the city of Kodiak (m)
1	Rupture model of the 1964 M_w 9.2 earthquake by Johnson and others (1996)	5–40	15–25	22.1	5.47	6.87	-0.18
2	M_w 9.1 earthquake in the area of Kodiak Island, 10 km depth	1–35	7.5–12.5	50.2	2.80	10.64	-2.18
3	M_w 9.0 earthquake in the area of Kodiak Island, 15 km depth	5–35	12.5–17.5	34.8	5.24	8.35	-3.98
4	M_w 9.0 earthquake in the area of Kodiak Island, 20 km depth	5–35	17.5–22.5	35.2	6.50	7.75	-5.42
5	M_w 9.0 earthquake in the area of Kodiak Island, 25 km depth	5–35	22.5–27.5	35.1	8.36	7.27	-7.07
6	M_w 9.1 earthquake in the area of Kodiak Island, 15–25 km depth	5–35	15–25	34.3	7.97	8.72	-7.02
7	M_w 9.1 earthquake in the area of Kodiak Island with a splay fault, 15–25 km depth	5–35	15–25	34.3	7.75	8.72	-6.62
8	M_w 9.2 earthquake in the area of Kodiak Island with 44 m of maximum slip	5–50	12–17	44.0	7.40	14.64	-2.25
9	M_w 9.25 earthquake in the area of Kodiak Island with 50 m of maximum slip	5–31	5–18	50.0	6.12	22.59	-3.38
10*	M_w 9.0–9.1 earthquake in the Cascadia subduction zone	Wang and others, 2003	Wang and others, 2003	35–45	7.50	10.90	0.00

Scenario 1: Repeat of the M_w 9.2 Great Alaska Earthquake

Currently, there are a few models of coseismic deformation for the M_w 9.2 Great Alaska Earthquake. The previous tsunami hazard assessment report by Suleimani and others (2002) employed the deformation model by Johnson and others (1996). After publication of the 2002 tsunami hazard assessment report, new deformation models for the 1964 event by Ichinose and others (2007), by Suito and Freymueller (2009), and by Suleimani (2011) became available. Our modeling results indicate that maximum wave height near Kodiak for the Johnson and others (1996) model is the highest among modeling results for other deformation models. Therefore, we employ the coseismic deformation model according to Johnson and others (1996) for the repeat of the 1964 event in Kodiak. We emphasize that in this study the model for the repeat of the M_w 9.2 Great Alaska Earthquake is the same as in the previous tsunami hazard assessment study. The slip at subfaults in the Prince William Sound region and along Kodiak Island is shown in figure 9a; vertical coseismic deformation for this scenario is shown in figure 10a.

In scenarios 2-5, we assume a maximum slip near the most sensitive areas for Chiniak Bay, i.e., at 10-20 km (6-12 mi) depth, or around cases C and D of the sensitivity study. We consider various downdip locations for the maximum slip in order to parameterize various credible tsunamigenic earthquakes. In the downdip direction, the slip is determined by the slip skewness parameter q in the Freund and Barnett (1976) formulae. For each scenario, the maximum slip is assumed to be located at a different depth. Unfortunately, a realistic, very complex slip distribution is not available from the Freund and Barnett (1976) formulae. We note that the presented scenarios try to capture the maximum credible scenarios and provide a starting point for development of more complex models.

Scenario 2: M_w 9.1 earthquake in the area of Kodiak Island; 10 km (6.2 mi) depth

This event is a hypothetical M_w 9.1 earthquake rupturing the Kodiak segment of the Aleutian megathrust with maximum slip at shallow depth. The slip skewness parameter, *q*, is set to 0.5 (symmetrical bell-shaped curve for the slip distribution) to model the maximum slip of 50 m (164 ft) at a depth of 10 km (6.2 mi) and corresponds to sensitivity case D. The updip and downdip limits of the rupture are 1 km (0.6 mi) and 35 km (21.7 mi), respectively. The proposed slip distribution is shown in figure 9b; vertical coseismic deformations for this scenario are shown in figure 10b.

Scenario 3: M_w 9.0 earthquake in the area of Kodiak Island; 15 km (9.3 mi) depth

This event is a hypothetical M_w 9.0 earthquake rupturing the Kodiak segment of the Aleutian megathrust. The depth of maximum slip is between the corresponding depths for sensitivity cases C and D. The slip skewness parameter, *q*, is set to 0.35 (bell-shaped curve skewed toward the trench) to model the maximum slip of 35 m (115 ft) at a depth of 15 km (9.3 mi). The updip and downdip limits of the rupture are 5 km (3.1 mi) and 35 km (21.7 mi), respectively. The proposed slip distribution is shown in figure 9c; vertical coseismic deformations for this scenario are shown in figure 10c.

Scenario 4: M_w 9.0 earthquake in the area of Kodiak Island, 20 km (12.4 mi) depth

This event is a hypothetical M_w 9.0 earthquake rupturing the Kodiak segment of the Aleutian megathrust. The depth of maximum slip corresponds to that for sensitivity case C. The slip skewness parameter, *q*, is set to 0.5 to model the maximum slip of 35 m (115 ft) at a depth of 20 km (12.4 mi). The updip and downdip limits of the rupture are 5 km (3.1 mi) and 35 km (21.7 mi), respectively. The proposed slip distribution is shown in figure 9d; vertical coseismic deformations for this scenario are shown in figure 10d.

Not to overlook other relevant scenarios between 5 km (3.1 mi) and 35 km (22 mi) depth, we include scenarios 5 and 6 with the maximum slip placed on both sides of the 20 km (12.4 mi) depth contour on the plate interface. The width of the high slip area is also increased to account for potential variations in the depth of the slip distribution.

Scenario 5: M_w 9.0 earthquake in the area of Kodiak Island, 25 km (15.5 mi) depth

This event is a hypothetical M_w 9.0 earthquake rupturing the Kodiak segment of the Aleutian megathrust. The depth of maximum slip is between the corresponding depths for sensitivity cases B and C. The slip skewness parameter, *q*, is set to 0.7 (bell-shaped curve skewed toward the deeper plate interface contours) to model the maximum slip of 35.1 m (115.2 ft) at a depth of 25 km (15.5 mi). The updip and downdip limits of the rupture are 5 km (3.1 mi) and 35 km (21.7 mi), respectively. The proposed slip distribution is shown in figure 9e; vertical coseismic deformations for this scenario are shown in figure 10e.

Scenario 6: M_w 9.1 earthquake in the area of Kodiak Island, 15–25 km (9.3–15.5 mi) depth

This event is a hypothetical M_w 9.1 earthquake rupturing the Kodiak segment of the Aleutian megathrust. The depth of maximum slip is 20 km (12.4 mi), which corresponds to sensitivity case C, but the width of the maximum slip of 34.3 m (112.5 ft) extends from the 15 to 25 km (9.3 to 15.5 mi) depth contours of the plate interface. The updip and downdip limits of the rupture are 5 km (3.1 mi) and 35 km (21.7 mi), respectively. The proposed slip distribution is shown in figure 9f; vertical coseismic deformations for this scenario are shown in figure 10f.

A number of studies published in the years following the 1964 earthquake analyzed data on coseismic displacements and land features associated with the system of splay faults, as well as tsunami arrival times and tsunami amplitudes along the coast of the Kenai Peninsula and Kodiak Island (Plafker, 1965, 1967, 1969; Plafker and others, 1969). Recently Liberty and others (2013) analyzed high-resolution seismic reflection data for the Prince William Sound area of the 1964 rupture and found that the greatest coseismic uplift in that region occurred on a series of splay faults.

Scenario 7: M_w9.1 earthquake in the area of Kodiak Island with splay fault, 15–25 km (9.3–15.5 mi) depth

In this scenario, we assume that the slip is partitioned between the megathrust and a splay fault offshore the easternmost tip of Kodiak Island. The considered splay fault follows the extent of the Narrow Cape fault and its involvement in the rupture is supported by evidence for slip on the Patton Bay fault system during the 1964 earthquake (Plafker, 1967).

The slip distribution for this scenario is the same as for scenario 6, but with an added splay fault with 10 m (32.8 ft) of slip. Parameters of the splay fault are listed in table 4. The depth of maximum slip is 20 km (12.4 mi), which corresponds to sensitivity case C, but the bandwidth of the maximum slip of 34.3 m (112.5 ft) extends from the 15 to 25 km (9.3–15.5 mi) depth contours of the plate interface. The updip and downdip limits of the rupture are 5 km (3.1 mi) and 35 km (21.7 mi), respectively. The proposed slip distribution is shown in figure 9g; vertical coseismic deformations for this scenario are shown in figure 10g.

Table 4. Fault parameters for scenario 7.

Latitude (°N)	Longitude (°W)	Depth (km)	Length (km)	Width (km)	Strike (deg.)	Dip (deg.)	Rake (deg.)	Slip (m)
57°53'35" N	151°17'57" W	0.5	75.93	31.6	226	60	90	10

Recently Butler and others (2014) described a layer of sand discovered in the Makauwahi sinkhole on the island of Kaua'i, Hawai'i. The origin of this layer is attributed to inundation of the sinkhole by a giant paleotsunami following a M_w 9+ earthquake in the eastern Aleutian Islands. Butler (2012) provides an in-depth examination of previous great Aleutian earthquakes and tsunamis impacting Hawai'i. In subsequent research Butler (2014) considered several hypothetical events with a 35 m (114.8 ft) displacement on the megathrust and up to a 50 m (164.0 ft) displacement near the trench. We assume that similar hypothetical events might occur near Kodiak Island and consider two additional scenarios.

Scenario 8: M_w 9.2 earthquake in the area of Kodiak Island with 44 m (144.4 ft) of maximum slip

In this scenario we assume 35 m (114.8 ft) slip on the plate interface and up to a 46 m (150.9 ft) slip near the trench. The slip is distributed almost uniformly along strike in the area of Kodiak Island except for the edges of the rupture, where it tapers. The proposed slip distribution is shown in figure 9h; vertical coseismic deformations for this scenario are shown in figure 10h. A similar scenario was proposed in the tsunami modeling study for Chignik (scenario 8 of Nicolsky and others, 2016).

Scenario 9: M_w9.25 earthquake in the area of Kodiak Island with 50 m (164.0 ft) of maximum slip

In this scenario, similar to Butler (2014), we assume 20 m (65.6 ft) slip on the plate interface between the 17.9 km (11.1 mi) and 30.8 km (19.1 mi) depth contours, and up to 50 m (164.0 ft) slip near the trench between 5 km (3.1 mi) and 17.9 km (11.1 mi) depth. The slip is distributed uniformly along strike in the area of Kodiak Island. The proposed slip distribution is shown in figure 9i; vertical coseismic deformations for this scenario are shown in figure 10i. A similar scenario was proposed in the tsunami modeling study for Chignik (scenario 7 of Nicolsky and others, 2016).

Although a rupture of the Cascadia subduction zone is not a worst-case scenario for the Kodiak area, for the sake of community preparedness we also simulate a large hypothetical earthquake along the western seaboard of the U.S.

Scenario 10: Rupture of the Cascadia subduction zone, including the entire megathrust between British Columbia and northern California

This scenario is the same as scenario 16 in the tsunami modeling studies for King Cove and Cold Bay (Suleimani and others, 2016). The slip distribution model for this scenario is shown in figure 10 of Wang and others (2003). The vertical coseismic deformations for this scenario are shown in figure 10j.

MODELING RESULTS

We performed numerical calculations for each of the ten hypothetical earthquake scenarios described above and summarized in table 3. Water dynamics are modeled for each grid listed in table 2; the extent of inundation and flow depths are calculated only for the level 4 high-resolution grid. Map sheets 1–5 show the maximum composite extent of inundation for all scenarios, and the maximum composite flow depths over dry land. The composite values are calculated as follows: for each tsunami scenario, the tsunami flow depth is computed at each grid point and at every time step during the tsunami propagation time, and the maximum value is kept; then we compute the composite maximum flow depth from all considered scenarios by again choosing the maximum value for each grid point among all scenarios. The same methodology is used to calculate the composite extent of tsunami inundation. The calculated extent of inundation accounts for coseismic deformation in the communities.

CITY OF KODIAK

The simulated extents of tsunami inundation in Kodiak for all scenarios are shown in figure 11. The extent of inundation corresponding to scenario 1, the repeat of the 1964 Great Alaska Earthquake, is very close to the 1964 observed inundation line. All other scenarios, except for scenario 10, which represents the far-field tsunami from the Cascadia Subduction zone, produce an inundation zone that exceeds the inundation caused by the 1964 tsunami. In scenarios 6 and 7, the simulated tsunami reaches as far as the intersection of Hemlock and Willow Streets. In the northeastern part of town around Mill Bay, scenarios 8 and 9 produce the largest inundation areas. Map sheets 2 and 3 show the composite inundation line and flow depths over dry land for the entire city. The downtown Kodiak area, harbor facilities, and the areas between and around Potatopatch and Mission Lakes are all inside the inundation zone, with flow depths reaching 13 m (42.7 ft). The numerical simulations reveal that for some scenarios the first wave could arrive at Kodiak about 40 minutes after the earthquake. As was demonstrated by the 1964 tsunami and also by the time series data shown in figure A-2, significant wave activity could continue in Kodiak for at least 12 hours after the earthquake, and the predicted average time interval between successive waves is 45 minutes to 1.5 hours.

U.S. COAST GUARD BASE

Figure 12 shows the simulated extents of tsunami inundation for all scenarios in the area of U.S. Coast Guard Base Kodiak. Scenario 1 produces a slightly larger inundation area than that observed in 1964. Similar to the downtown area, the worst-case scenarios in this area are scenarios 6 and 7. In all scenarios, the airport landing strips are flooded to some extent. The area that is not inundated by any of the simulated scenarios is the hill adjacent to the airport, between Albatross Avenue and Polaris Avenue. Map sheet 4 shows the composite inundation line and flow depths over dry land for the entire base. The airport landing strips, the hangars, and other base facilities are inside the inundation zone, with flow depths ranging from 5 to 15 m (16.4 to 49.2 ft). The time series for points 5 and 6 in figure A-2 show that waves as high as 10 m (32.8 ft) could keep arriving for about six hours, at 1- to 1.5-hour intervals.

WOMENS BAY

The simulated extents of tsunami inundation in the community of Womens Bay for all scenarios are shown in figure 13. The far-field Cascadia tsunami (scenario 10) is the only scenario that does not completely flood West Rezanof Drive, the road that connects the community to the Coast Guard base; all other scenarios inundate the road. Even though scenario 6 produces the largest inundation area, three other scenarios (3, 4, and 5) generate quite similar results because of the area's low elevation. Map sheet 5 shows the composite inundation line and flow depths over dry land for Womens Bay. The results indicate that a substantial part of the community at lower elevations is inside the inundation zone, with flow depths ranging from 3 to 13 m (9.8 to 42.7 ft). The time series data for point 3 (West Rezanof Drive, appendix A-1) in figure A-2 show that waves as high as 6 m (19.7 ft) could overflow the road for about six hours at 1- to 1.5-hour intervals.

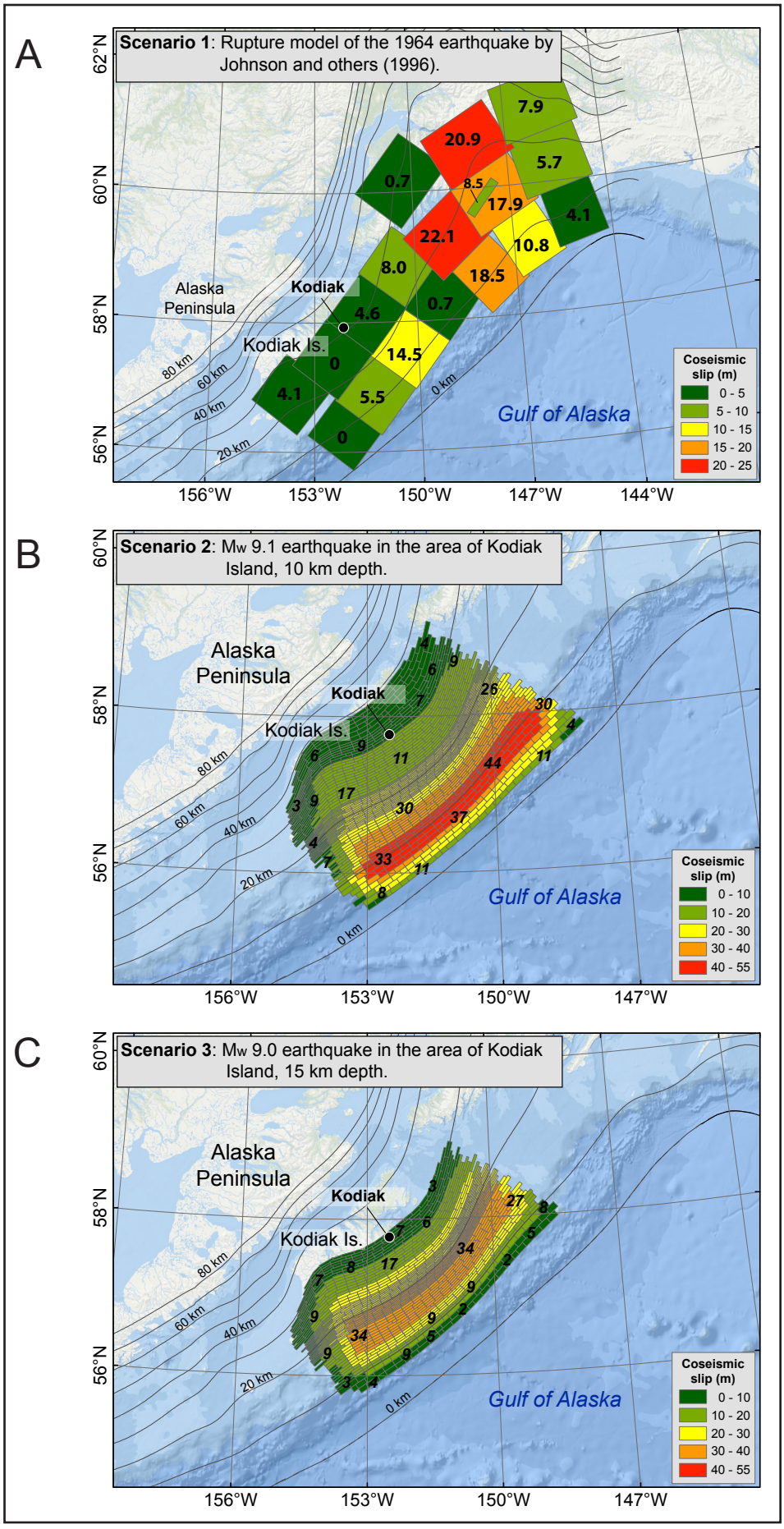

Figure 9. Estimated slip distributions along the plate interface for scenarios 1–9. Slip values (in meters) are identified by small black labels. Depth contours of the Aleutian subduction interface are shown by heavy black lines. Slip distribution is not provided for scenario 10.

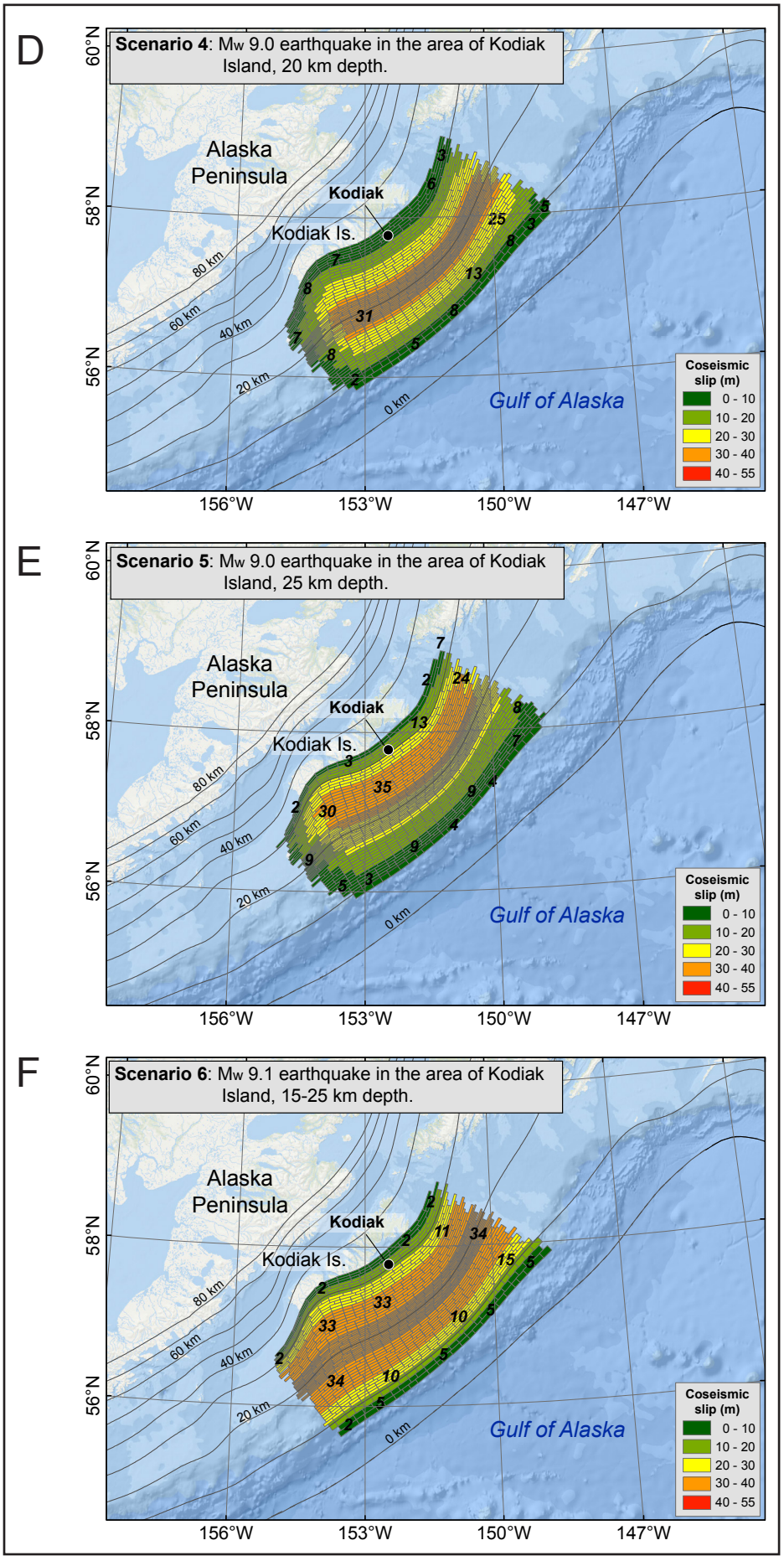

Figure 9, continued. Estimated slip distributions along the plate interface for scenarios 1–9. Slip values (in meters) are identified by small black labels. Depth contours of the Aleutian subduction interface are shown by heavy black lines. Slip distribution is not provided for scenario 10.

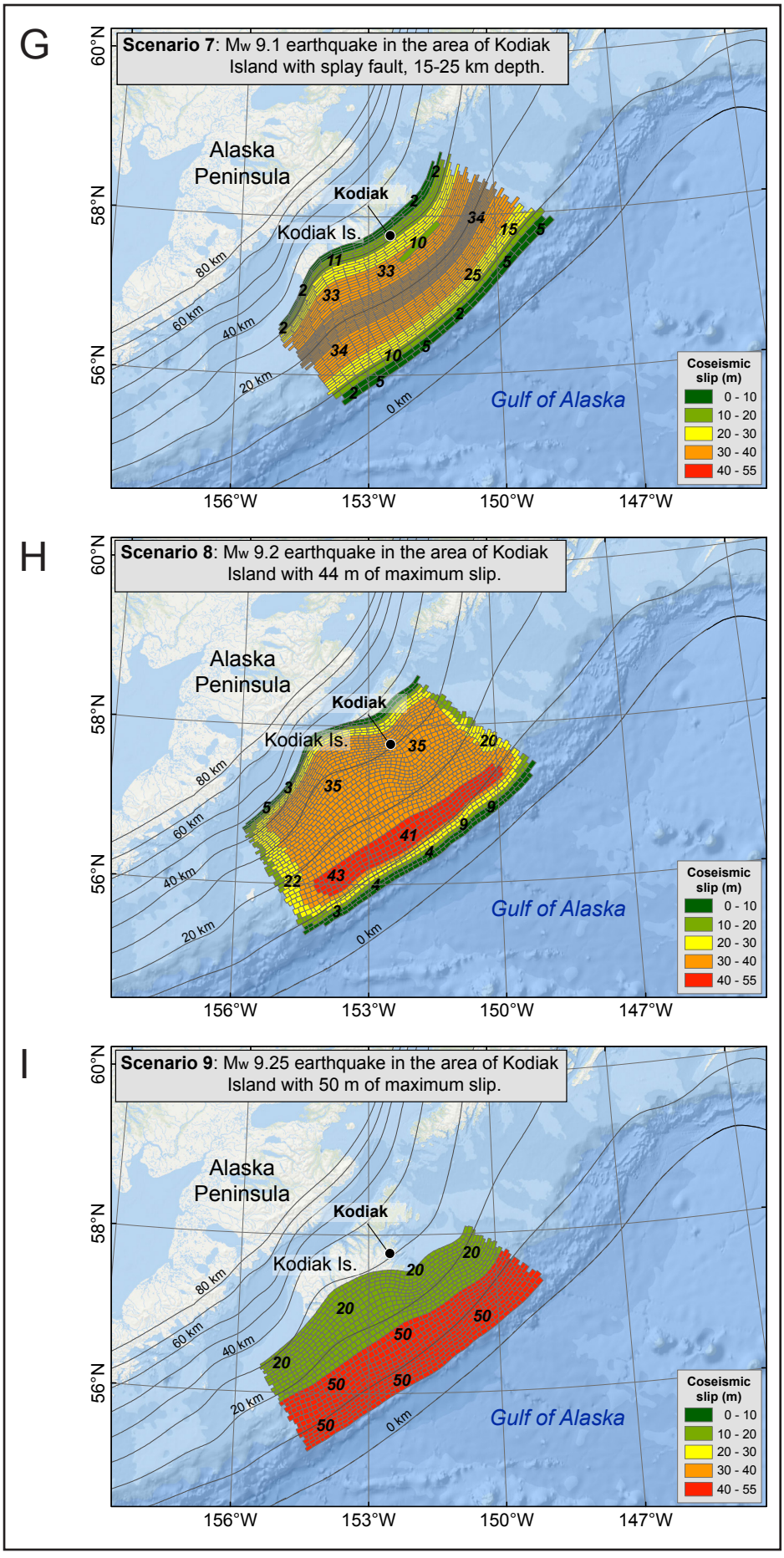

Figure 9, continued. Estimated slip distributions along the plate interface for scenarios 1–9. Slip values (in meters) are identified by small black labels. Depth contours of the Aleutian subduction interface are shown by heavy black lines. Slip distribution is not provided for scenario 10.

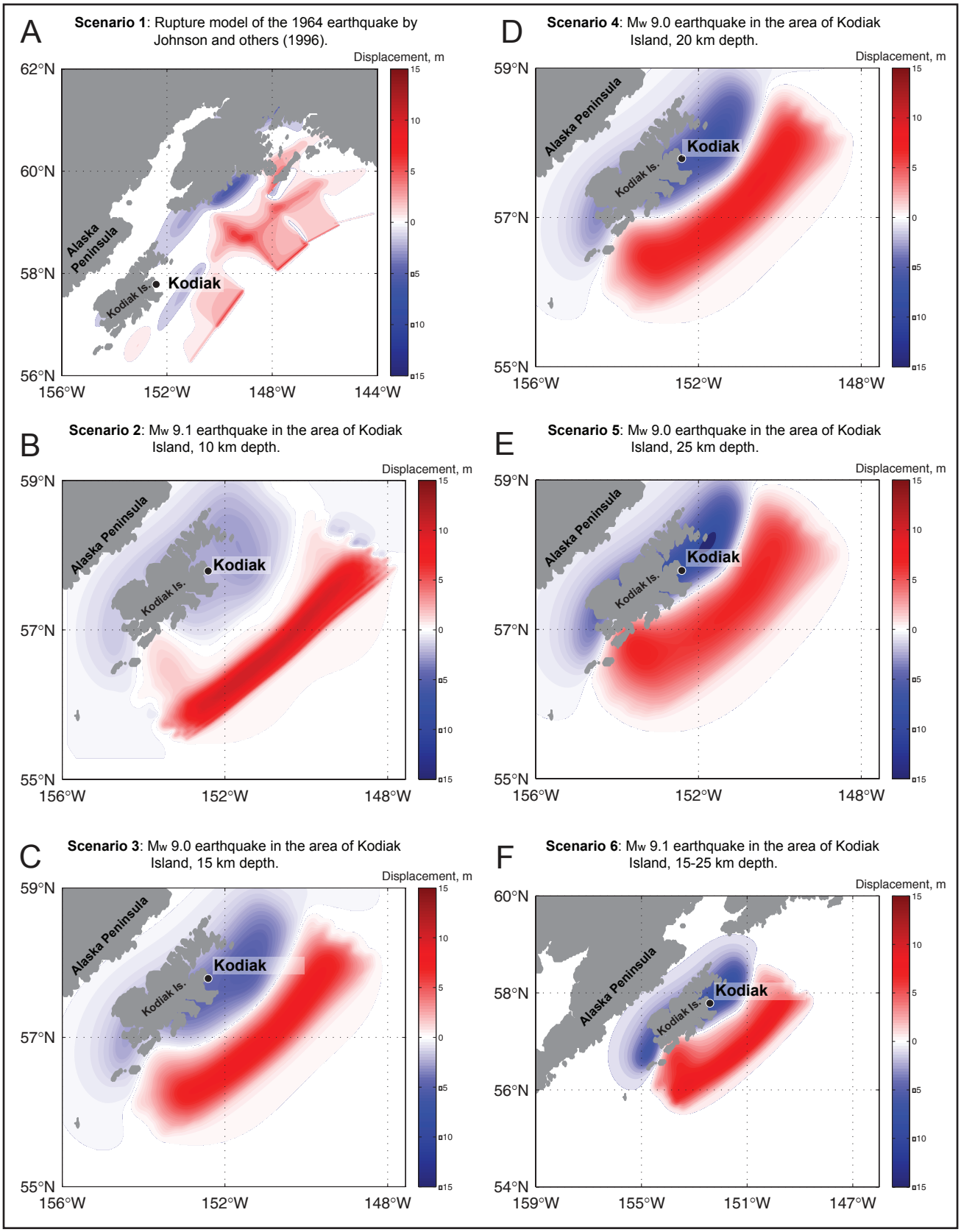

Figure 10. Computed vertical surface deformation related to the proposed slip distributions shown in figure 9. Blue shaded areas are associated with coseismic ground subsidence; areas of uplift are shown in red.

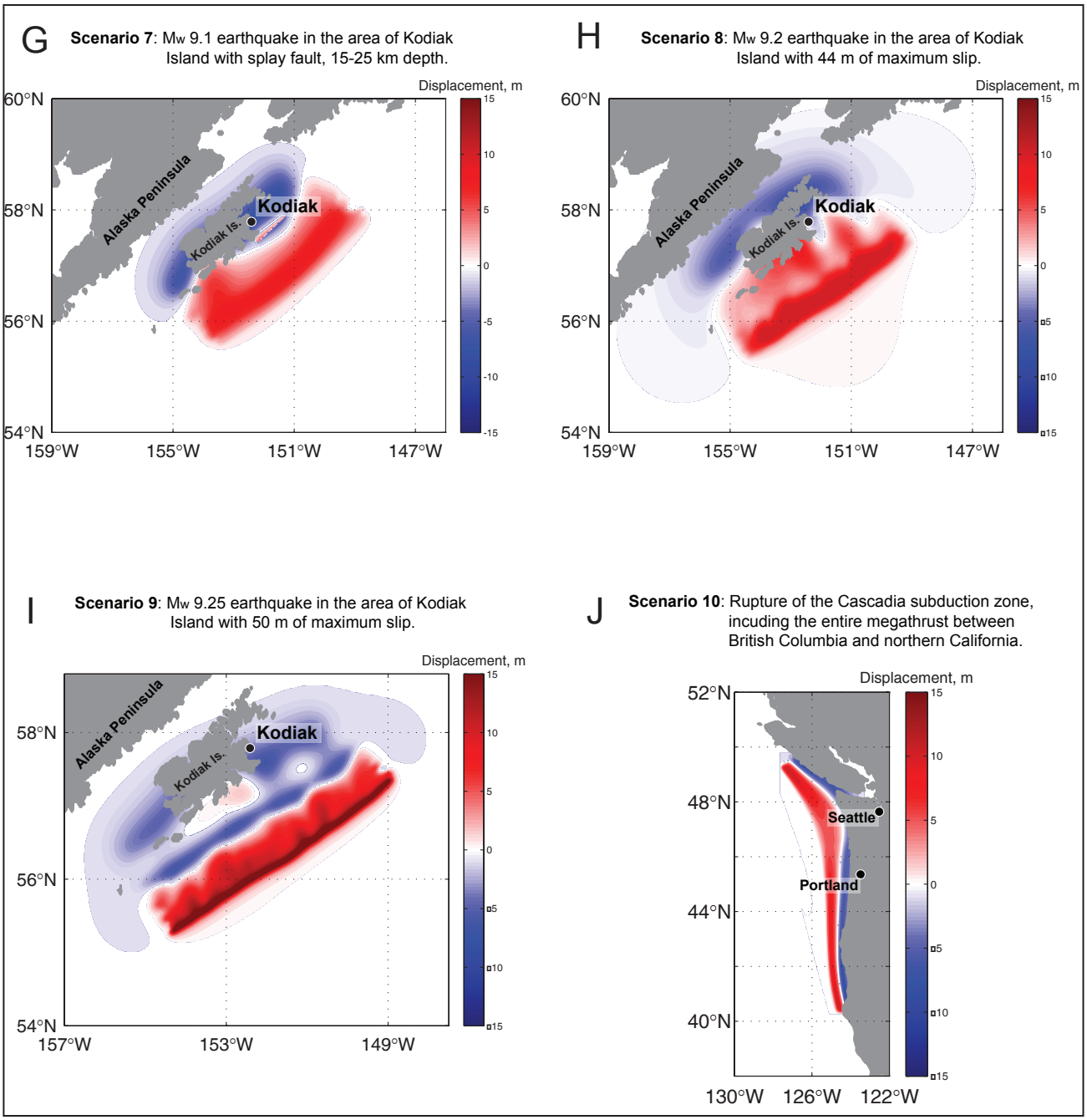

Figure 10, continued. Computed vertical surface deformation related to the proposed slip distributions shown in figure 9. Blue shaded areas are associated with coseismic ground subsidence; areas of uplift are shown in red.

TIME SERIES AND OTHER NUMERICAL RESULTS

To help emergency managers assess tsunami hazard in the communities, we supplement the inundation maps with the time series of the modeled water level and velocity dynamics at certain locations around Chiniak Bay. The arrival time of the first wave, the maximum wave amplitude, and the duration of wave action are all important factors that should be considered by emergency managers during evacuation planning. Appendix A contains plots of sea level and velocity time series for selected scenarios at critical locations. For each location shown by a number in figure A-1, we plot the sea level and water velocity in figure A-2 for selected scenarios (scenarios 1, 4, 6, 8, and 9). Scenarios 2–5 were derived from the sensitivity study and have similar parameters except for the depth of maximum slip. Therefore we plot the results only for scenario 4 from this group of scenarios, as it simulates the highest wave. Scenarios 6 and 7 differ only by the added splay fault in scenario 7 and produce quite similar results, so we provide time series for scenario 6 only. Scenario 6 simulates the highest wave and is considered the worst-case scenario for all three communities. The splay fault in

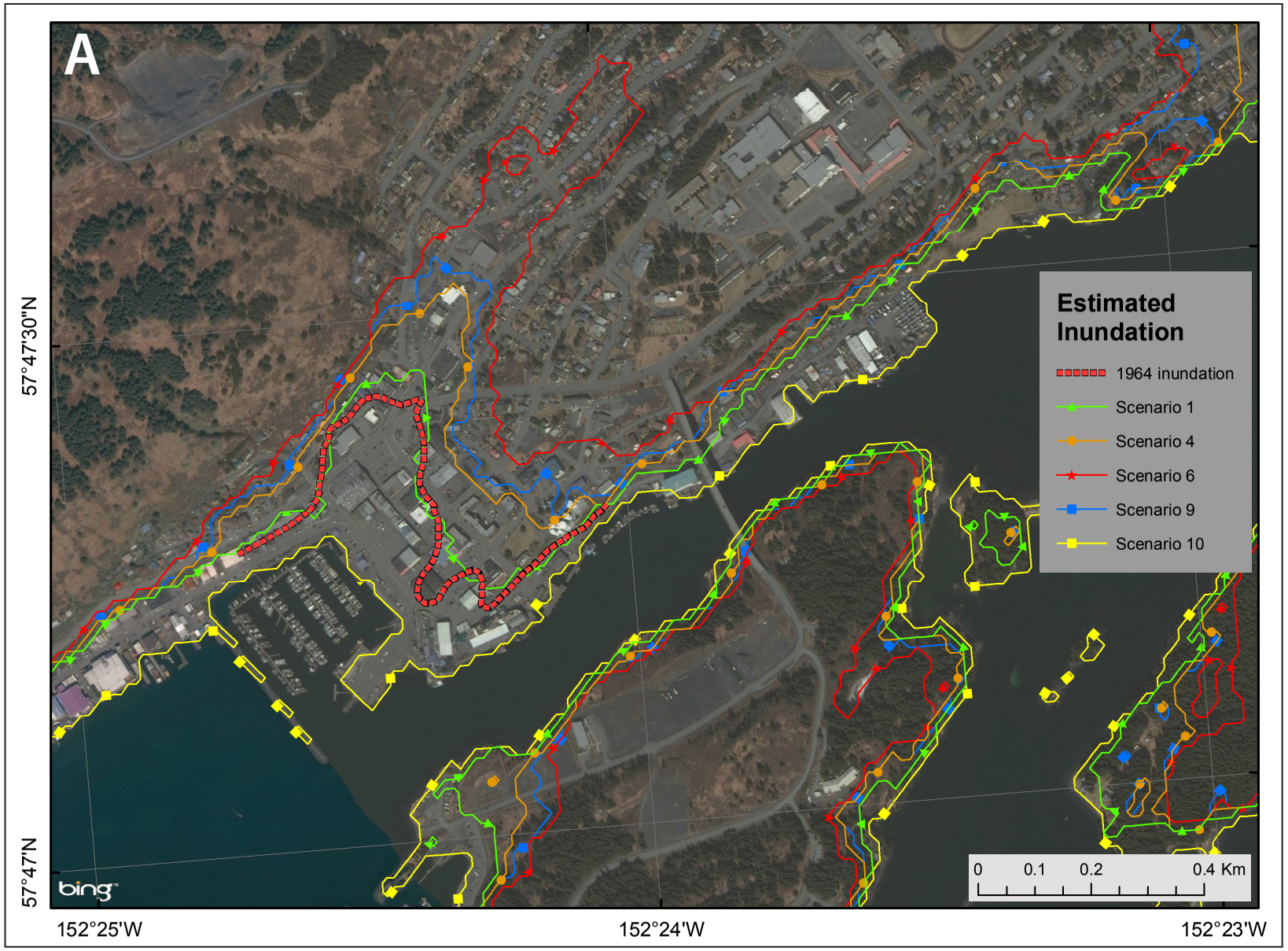

Figure 11. Modeled potential inundation for (a) downtown Kodiak for selected scenarios. The dashed red line represents the observed inundation extent of the 1964 tsunami. Since the mapped extent of the 1964 inundation was limited, this line does not occur everywhere. Because of the steep topography, inundation areas for several tsunami scenarios may have a common boundary, and the plotted extents of the inundation areas may overlie each other in places.

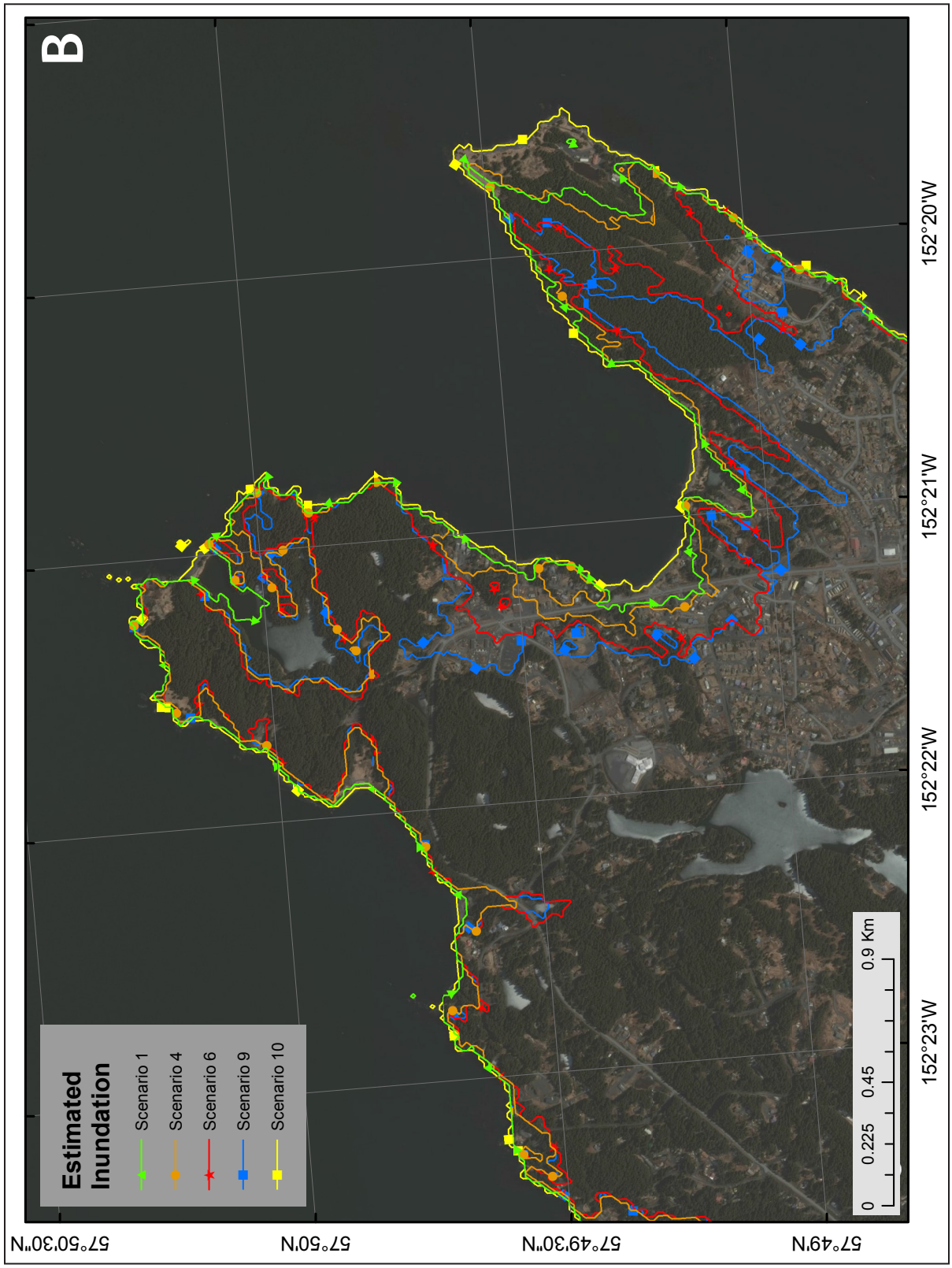

Figure 11, continued. Modeled potential inundation for (B) the northeastern part of Kodiak by tectonic tsunami waves for selected scenarios. Because of the steep topography, inundation areas for several tsunami scenarios may have a common boundary, and the plotted extents of the inundation areas may overlie each other in places.

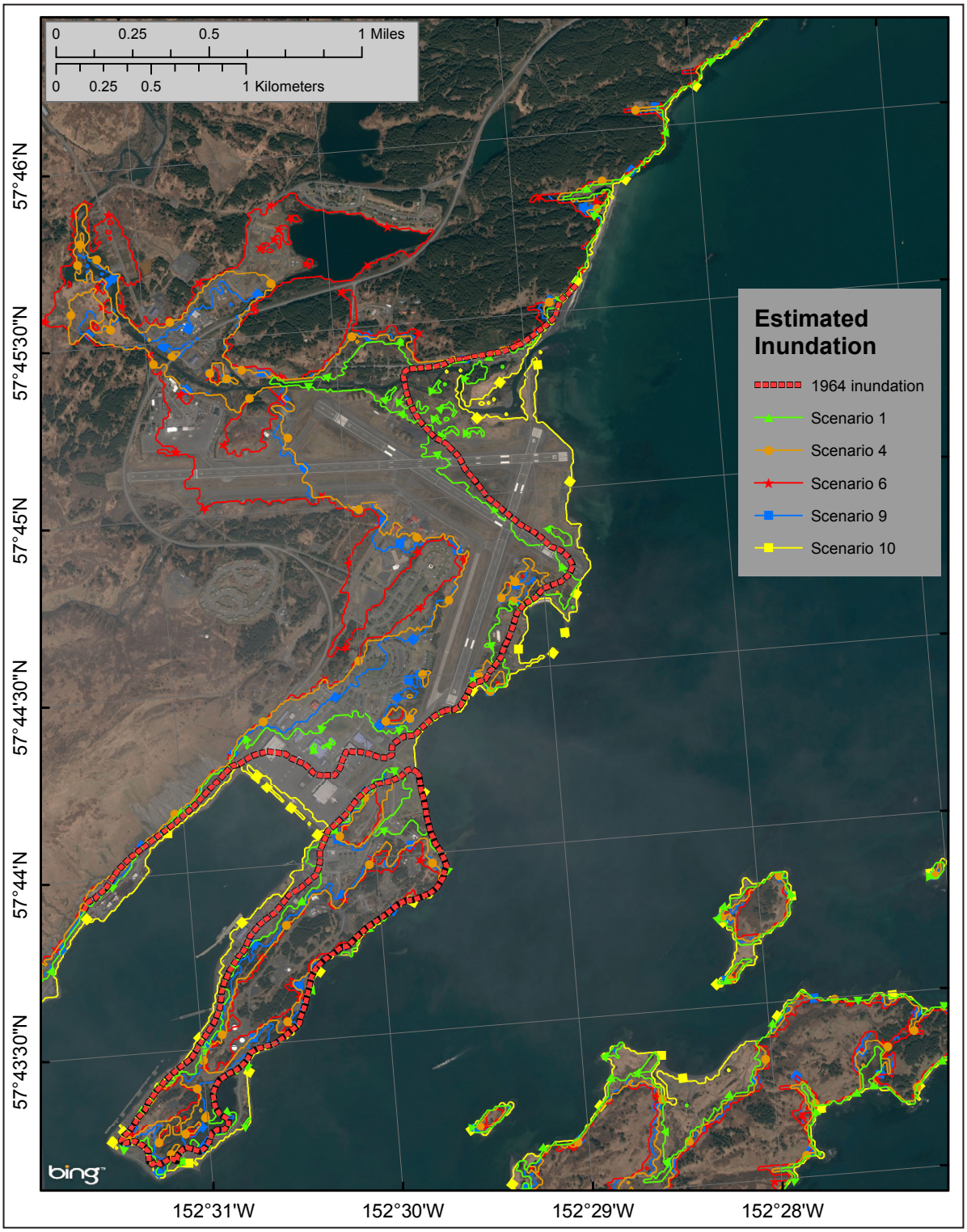

Figure 12. Modeled potential inundation for U.S. Coast Guard Base Kodiak by tectonic waves for selected scenarios. The dashed red line represents the observed inundation extent of the 1964 tsunami. Since the mapped extent of the 1964 inundation was limited, this line does not occur everywhere. Because of the steep topography, inundation areas for several tsunami scenarios may have a common boundary and the plotted extents of the inundation areas may overlie each other in places.

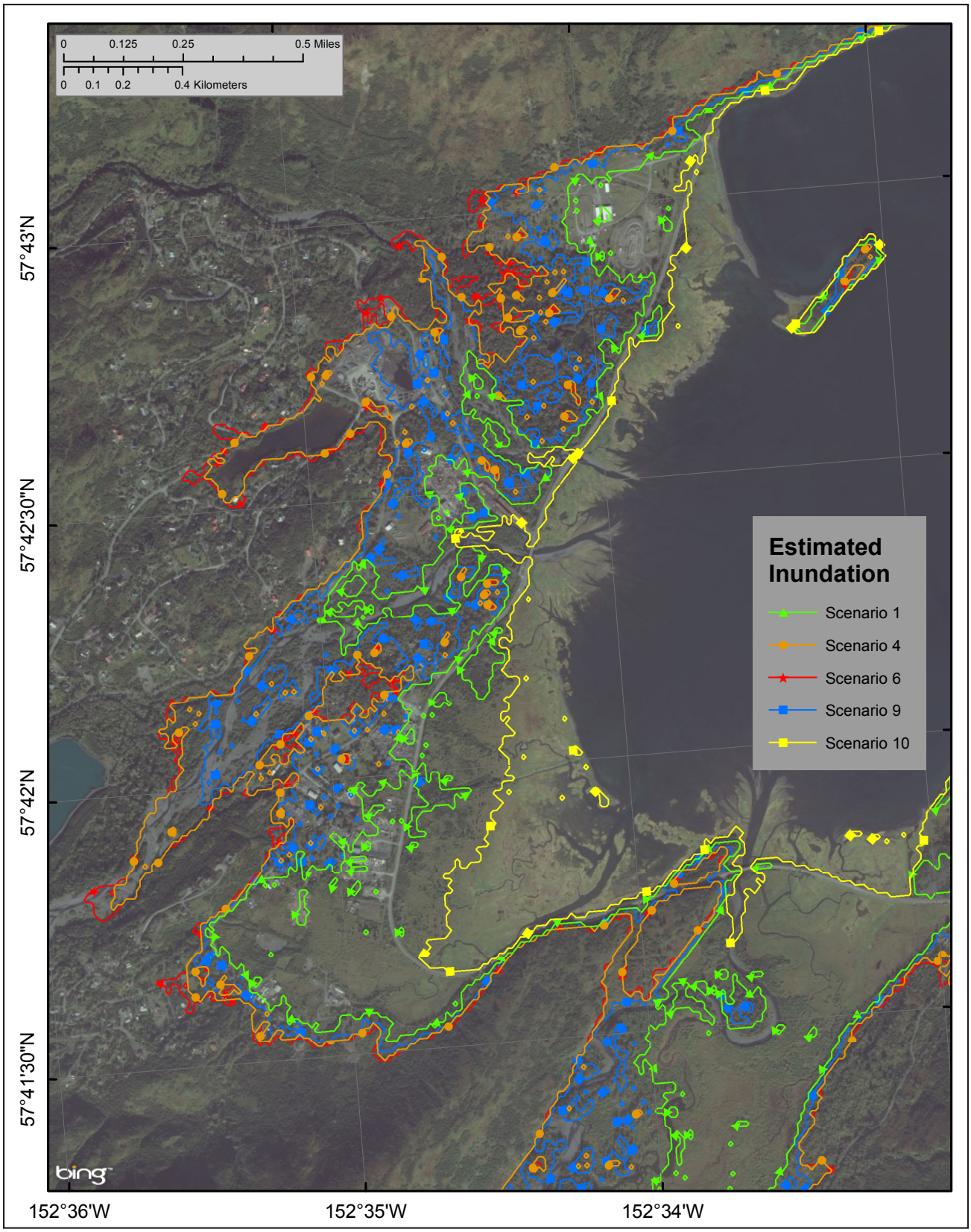

Figure 13. Modeled potential inundation in Womens Bay by tectonic waves for selected scenarios. Because of the steep topography, inundation areas for several tsunami scenarios may have a common boundary and the plotted extents of the inundation areas may overlie each other in places.

scenario 7 produces uplift in the general area of subsidence that is caused by slip on the megathrust, and therefore reduces the amount the subsidence around Kodiak. That resulted in a slightly smaller wave height in scenario 7 compared to scenario 6. Scenario 10 is the far-field event for Kodiak, which results in minimal inundation in all locations and is thus not included.

In all plots in Appendix A, zero time corresponds to the time when the earthquake occurs. The pre-earthquake elevation/depth with respect to the MHHW is stated for each location. The post-earthquake elevation/depth corresponding to the MHHW datum is also listed for each scenario. To show the height of arriving tsunamis for offshore locations, we use a vertical datum with a zero mark corresponding to the pre-earthquake sea level. The dashed lines show water levels after the tsunami. The velocity magnitude is calculated as water flux divided by water depth, thus the velocity value can have large uncertainties when the water depth is small. In the plots provided, the velocity is computed only where the water depth is greater than 0.3 m (1.0 ft).

Analysis of the time series plot shows that a hypothetical earthquake with a magnitude of 9.0–9.1 could cause devastating waves that would inundate significant areas in all three communities. The maximum water level and velocity for all considered scenarios are listed in appendix tables A-1 and A-2, respectively.

In addition to the time series of the modeled water level and velocity dynamics, we have also modeled the potential maximum subsidence in the Kodiak area and generated maps of permanent flooding associated with the various scenarios (map sheets 6-10). Scenarios 5 and 6 result in the maximum subsidence in the city of Kodiak---about 7 m (23 ft). Most low-lying areas could be permanently flooded as a result of these hypothetical earthquakes.

SOURCES OF ERRORS AND UNCERTAINTIES

The hydrodynamic model used to calculate propagation and runup of tsunami waves is a nonlinear, flux-formulated, shallow-water model (Nicolsky and others, 2011b) that has passed the validation and verification tests required for models used in production of tsunami inundation maps (Synolakis and others, 2007; National Tsunami Hazard Mitigation Program [NTHMP], 2012). The uncertainties in tsunami modeling include bottom friction, presence or absence of buildings and vegetation in DEMs, the time delay between the observed and computed tsunami arrivals discussed above, the lack of horizontal deformation in the displacement models, and assumption of instantaneous displacement. The tsunami scenarios that we calculate in this report are considered to be sufficient to capture the worst-case tsunami event, but there are still an infinite number of possible slip distributions. Further details about the limitations of the employed modeling approach are described in earlier reports by Suleimani and others (2010, 2013, 2015) and Nicolsky and others (2011a, 2011b, 2013, 2014, 2015), as well as in NTHMP (2012). The accuracy of the later waves is limited by the accuracies of the bathymetry and coastline that are outside the extent of the high-resolution DEM but still impact the modeling.

SUMMARY

We present the results of numerical modeling of earthquake-generated tsunamis for the communities of the city of Kodiak, U.S. Coast Guard Base Kodiak, and Womens Bay on Kodiak Island, Alaska. The earthquake scenarios considered in this report include a range of magnitudes for ruptures on the Kodiak Island segment of the Aleutian megathrust. Hypothetical scenarios 6 and 7 (M_w9.1 earthquakes in the area of Kodiak Island with maximum slip distributed between the 15 and 25 km [9.3–15.5 mi] depth) result in the "worst case" tsunami-inundation hazards for the Kodiak Island communities. The results show that the maximum predicted flow depth in downtown Kodiak can reach 13 m (42.7 ft), and the currents in Kodiak's Inner Harbor can be as strong as 3.7 m/sec (7.2 knots). Dangerous wave activity is expected to last for at least 10 hours after the earthquake.

Each of the scenarios considered are geologically reasonable and present potential hazards to the communities. Map sheets 1–3, showing the potential extent of inundation and the tsunami flow depths, have been completed using the best information available and are believed to be accurate; however, their preparation required many assumptions. We considered a suite of tectonic scenarios and provide an estimate of maximum credible tsunami inundation for each scenario. Actual conditions during a tsunami event could vary from the scenarios considered in this report, which are not intended to predict future tsunamis. Instead, the scenarios described are used to estimate the variability of possible outsized earthquakes that may produce something near to maximum tsunami inundations. The limits of inundation shown should be used only as a guideline for emergency planning and response action. Actual areas inundated will depend on specifics of earth deformation, land construction, and tide level, and may differ from areas shown on the map. The information on this map is intended to assist state and local agencies in planning emergency evacuation and tsunami response actions in the event of a major tsunamigenic earthquake. These results are not intended for land-use regulation or building-code development.

ACKNOWLEDGMENTS

This report was funded by the U.S. Department of Commerce/National Oceanic and Atmospheric Administration (NOAA) through National Tsunami Hazard Mitigation Program Award NA15NWS4670027 to Alaska Division of Homeland Security and Emergency Management and University of Alaska Fairbanks. This does not constitute an endorsement by NOAA. Numerical calculations for this work were supported by High Performance Computing (HPC) resources at the Research Computing Systems unit at the Geophysical Institute, University of Alaska Fairbanks. We thank Robert Witter for his incredibly comprehensive review that helped improve the report, and Edison Gica for a number of insightful comments and suggestions.

REFERENCES

Briggs, R.W., Engelhart, S.E., Nelson, A.R., Dura, T., Kemp, A.C., Haeussler, P.J., Corbett, D.R., Angster, S.J., and Bradley, L.-A., 2014, Uplift and subsidence reveal a nonpersistent megathrust rupture boundary (Sitkinak Island, Alaska): Geophysical Research Letters, v. 41, no. 7, p. 2,289–2,296. http://doi.org/10.1002/2014GL059380

Butler, Rhett, 2012, Re-examination of the potential for great earthquakes along the Aleutian island arc with implication for tsunamis in Hawai'i: Seismological Research Letters, v. 83, no. 1, p. 30–39. http://doi.org/10.1785/gssrl.83.1.29

Butler, Rhett, 2014, Great Aleutian tsunamis: Honolulu, HI, University of Hawai'i at Manoa, Hawai'i Institute of Geophysics & Planetology, Peer-Reviewed Report HIGP-2014-1, 170 p., www.higp.hawaii.edu/reports/2014

Butler, Rhett, Burney, David, and Walsh, David, 2014, Paleotsunami evidence on Kaua'i and numerical modeling of a great Aleutian tsunami: Geophysical Research Letters, v. 41, no. 19, p. 6,795–6,802. http://doi.org/10.1002/2014GL061232

Carignan, K.S., McLean, S.J., Eakins, B.W., Love, M.R., and Sutherland, M., 2013, Digital elevation models of Kodiak, Alaska—Procedures, data sources, and analysis: Boulder, CO, NOAA National Centers for Environmental Information (NCEI). www.ngdc.noaa.gov/dem/report/download/5055

Carver, G.A., and Plafker, George, 2008, Paleoseismicity and neotectonics of the Aleutian subduction zone—An overview, *in* Freymueller, J.T., Haeussler, P.J., Wesson, R.L, and Ekström, G., eds., Active tectonics and seismic potential of Alaska: American Geophysical Union Geophysical Monograph 179, p. 43–63.

Christensen, D.H., and Beck, S.L., 1994, The rupture process and tectonic implications of the Great 1964 Prince William Sound Earthquake: Pure and Applied Geophysics, v. 142, no. 1, p. 29–53. http://doi.org/10.1007/BF00875967

DeMets, Charles, Gordon, R.C., Argus, D.F., and Stein, Seth, 1990, Current plate motions: Geophysical Journal International, v. 101, no. 2, p. 425–478. http://doi.org/10.1111/j.1365-246X.1990.tb06579.x

Department of Commerce, Community, and Economic Development (DCCED)/Division of Community and Regional Affairs (DCRA), 2015, Community Database Online, accessed November 22, 2016. https://www.commerce.alaska.gov/dcra/DCRAExternal

Dunbar, P.K., and Weaver, C.S., 2008, U.S. states and territories national tsunami hazard assessment—Historical record and sources for waves: Technical Report, National Oceanic and Atmospheric Administration and U.S. Geological Survey, 59 p. http://nthmp.tsunami.gov/documents/Tsunami_Assessment_Final.pdf

Eberhart-Phillips, D., Christensen, D.H., Brocher, T.M., Hansen, Roger, Ruppert, N.A., Haeussler, P.J., and Abers, G.A., 2006, Imaging the transition from Aleutian subduction to Yakutat collision in central Alaska, with local earthquakes and active source data: Journal of Geophysical Research, v. 111, no. B11, p. 303. http://doi.org/10.1029/2005JB004240

Ferris, Aaron, Abers, G.A., Christensen, D.H., and Veenstra, Elizabeth, 2003, High resolution image of the subducted Pacific(?) plate beneath central Alaska, 50–150 km depth: Earth and Planetary Science Letters, v. 214, no. 3-4, p. 575–588. http://doi.org/10.1016/S0012-821X(03)00403-5

Freund, L.B., and Barnett, D.M., 1976, A two-dimensional analysis of surface deformation due to dip-slip faulting: Bulletin of the Seismological Society of America, v. 66, no. 3, p. 667–675.

Freymueller, J.T., Woodard, H., Cohen, S., Cross, R., Elliott, H., Larsen, C., Hreinsdottir, S., and (Geophys. Monogr. Ser., 179, C. Zweck), Active deformation processes in Alaska, based on 15 years of GPS measurements, *in* Active Tectonics and Seismic Potential of Alaska, Geophys. Monogr. Ser., edited by J. T. Freymueller , P. J. Haeussler, R. Wesson, and G. Ekstrom, AGU, Washington, D. C., p. 1-42.

Gulick, S.P.S., Reece, R.S., Christenson, G.L., Van Avendonk, H.J.A., Worthington, L.L., and Pavlis, T.L., 2013, Seismic images of the Transition fault and the unstable Yakutat–Pacific–North American triple junction: Geology, v. 41, no. 5, p. 571–574. http://doi.org/10.1130/G33900.1

Holdahl, S.R., and Sauber, Jeanne, 1994, Coseismic slip in the 1964 Prince William Sound earthquake—A new geodetic inversion: Pure and Applied Geophysics, v. 142, no. 1, p. 55–82.

Ichinose, Gene, Somerville, Paul, Thio, H.K., Graves, Robert, and O'Connell, Dan, 2007, Rupture process of the 1964 Prince William Sound, Alaska, earthquake from the combined inversion of seismic, tsunami, and geodetic data: Journal of Geophysical Research, v. 112, no. B07, p. 306, 21 p., http://doi.org/10.1029/2006JB004728

Johnson, J.M., Satake, Kenji, Holdahl, S.R., and Sauber, Jeanne, 1996, The 1964 Prince William Sound earthquake—Joint inversion of tsunami waveforms and geodetic data: Journal of Geophysical Research, v. 101, no. B1, p. 523–532. http://doi.org/10.1029/95JB02806

Kachadoorian, Reuben, and Plafker, George, 1967, Effects of the earthquake of March 27, 1964, on communities of Kodiak Area: U.S. Geological Survey Professional Paper 542-F, 41 p. http://pubs.usgs.gov/pp/0542f/

Kachadoorian, Reuben, and Slater, W.H., 1978, Pillar Mountain landslide, Kodiak, Alaska: U.S. Geological Survey Open-File Report 78-217, 21 p., 2 sheets, scale 1 inch = 200 feet.

Kanamori, Hiroo, 1970, The Alaska earthquake of 1964—Radiation of long-period surface waves and source mechanism: Journal of Geophysical Research, v. 75, no. 26, p. 5,029–5,040. http://doi.org/10.1029/JB075i026p05029

Kirby, Stephen, Scholl, David, von Huene, Roland, and Wells, Ray, 2013, Alaska earthquake source for the SAFRR tsunami scenario, chapter B, *in* Ross, S.L., and Jones, L.M., eds., The SAFRR (Science Application for Risk Reduction) Tsunami Scenario: U.S. Geological Survey Open-File Report 2013–1170, 40 p. http://pubs.usgs.gov/of/2013/1170/b/

Kulikov, E.A., Rabinovich, A.B., Fine, I.V., Bornhold, B.D., and Thomson, R.E., 1998, Tsunami generation by landslides at the Pacific coast of North America and the role of tides: Oceanology, v. 38, no. 3, p. 323–328.

Lander, J.F., 1996, Tsunamis affecting Alaska, 1737–1996: Boulder, CO, National Oceanic and Atmospheric Administration, National Geophysical Data Center (NGDC), Key to Geophysical Research Documentation, v. 31, 155 p. ftp://ftp.ngdc.noaa.gov/hazards/publications/Kgrd-31.pdf

Lee, H.J., Ryan, Holly, Kayen, R.E., Haeussler, P.J., Dartnell, Peter, and Hampton, M.A., 2006, Varieties of submarine failure morphologies of seismically-induced landslides in Alaskan fjords: Norwegian Journal of Geology (Norsk Geologisk Tidsskrift), v. 86, no. 3, p. 221–230.

Liberty, L.M., Finn, S.P., Haeussler, P.J., Pratt, T.L., and Peterson, A., 2013, Megathrust splay faults at the focus of the Prince William Sound asperity, Alaska, Journal of Geophysical Research, 118, p. 1–14. http://doi.org/10.1002/jgrb.50372

Lim, E., Eakins, B.W., and Wigley, R., 2009, Southern Alaska coastal relief model—Procedures, data sources, and analysis: National Geophysical Data Center, NOAA, 25 p., http://www.ngdc.noaa.gov/mgg/coastal/s_alaska.html

National Centers for Environmental Information (NCEI/WDS), in progress, Global historical tsunami database at NCEI, 2100 BC to present (interactive map): National Centers for Environmental Information, NOAA, http://doi.org/10.7289/V5PN93H7

National Tsunami Hazard Mitigation Program (NTHMP), 2010, Guidelines and best practices for tsunami inundation modeling for evacuation planning: National Oceanic and Atmospheric Administration (NOAA), NTHMP Mapping & Modeling Subcommittee.

———2012, Proceedings and results of the 2011 NTHMP Model Benchmarking Workshop: Boulder, CO, U.S. Department of Commerce/NOAA/NTHMP, NOAA Special Report, 436 p. http://nthmp.tsunami.gov

Nicolsky, D.J., Suleimani, E.N., Combellick, R.A., and Hansen, R.A., 2011a, Tsunami inundation maps of Whittier and western Passage Canal, Alaska: Alaska Division of Geological & Geophysical Surveys Report of Investigation 2011-7, 65 p. http://doi.org/10.14509/23244

Nicolsky, D.J., Suleimani, E.N., Freymueller, J.T., and Koehler, R.D., 2015, Tsunami inundation maps of Fox Islands communities, including Dutch Harbor and Akutan, Alaska: Alaska Division of Geological & Geophysical Surveys Report of Investigation 2015-5, 67 p., 2 sheets, scale 1:12,500. http://doi.org/10.14509/29414

Nicolsky, D.J., Suleimani, E.N., and Hansen, R.A., 2011b, Validation and verification of a numerical model for tsunami propagation and runup: Pure and Applied Geophysics, v. 168, no. 6, p. 1,199–1,222. http://doi.org/10.1007/s00024-010-0231-9

Nicolsky, D.J., Suleimani, E.N., Haeussler, P.J., Ryan, H.F., Koehler, R.D., Combellick, R.A., and Hansen, R.A., 2013, Tsunami inundation maps of Port Valdez, Alaska: Alaska Division of Geological & Geophysical Surveys Report of Investigation 2013-1, 77 p., 1 sheet, scale 1:12,500. http://doi.org/10.14509/25055

Nicolsky, D.J., Suleimani, E.N., and Koehler, R.D., 2014, Tsunami inundation maps of Cordova and Tatitlek, Alaska: Alaska Division of Geological & Geophysical Surveys Report of Investigation 2014-1, 49 p. http://doi.org/10.14509/27241

———2016, Tsunami inundation maps for the communities of Chignik and Chignik Lagoon, Alaska: Alaska Division of Geological & Geophysical Surveys Report of Investigation 2016-8, 48 p., 2 sheets, scale 1:12,500. http://doi.org/10.14509/29675

Nishenko, S.P., 1991, Circum-Pacific seismic potential, 1989–1999: Pure and Applied Geophysics, v. 135, no. 2, p. 169–259. http://doi.org/10.1007/BF00880240

Nishenko, S.P., and Jacob, K.H., 1990, Seismic potential of the Queen Charlotte–Alaska–Aleutian seismic zone: Journal of Geophysical Research, v. 95, no. B3, p. 2,511–2,532. http://doi.org/10.1029/JB095iB03p02511

Plafker, George, 1965, Tectonic deformation associated with the 1964 Alaska earthquake: Science, v. 148, no. 3,678 p. 1,675–1,687.

Plafker, George, 1967, Surface faults on Montague Island associated with the 1964 Alaska earthquake: U.S. Geological Survey Professional Paper 543-G, p. G1–G42. http://pubs.usgs.gov/pp/0543g/

Plafker, George, 1969, Tectonics: U.S. Geological Survey Professional Paper 543-I, p. G1–G74.

Plafker, George, and Kachadoorian, Reuben, 1966, Geologic effects of the March 1964 earthquake and associated seismic sea waves on Kodiak and nearby islands, Alaska: U.S. Geological Survey Professional Paper 543–D, 46 p. http://pubs.usgs.gov/pp/0543d/

Plafker, George, Kachadoorian, Reuben, Eckel, E.B., and Mayo, L.R., 1969, Effects of the earthquake of March 27, 1964, on various communities: U.S. Geological Survey Professional Paper 542-G, 50 p. http://pubs.usgs.gov/pp/0542g/

Ross, S.L., and Jones, L.M., eds., 2013, The SAFRR Tsunami Scenario: U.S. Geological Survey Open-File Report 2013–1170, 897 p. http://pubs.usgs.gov/of/2013/1170/

Schlotfeldt, P., Tart, R. Jr., Panton, B., and Dugan, R., 2014, Pillar Mountain landslide—Failure mechanism update: American Rock Mechanics Association, Proceedings of the 48th U.S. Rock Mechanics/Geomechanics Symposium, June 1–4, 2014.

Shao, Guangfu, Li, Xiangyu, Ji, Chen, and Maeda, Takahiro, 2011, Focal mechanism and slip history of 2011 M_w 9.1 off the Pacific coast of Tohoku earthquake, constrained with teleseismic body and surface waves: Earth Planets and Space, v. 63, no. 7, p. 559–564. http://doi.org/10.5047/eps.2011.06.028

Shennan, Ian, Barlow, Natasha, Carver, Gary, Davies, Frank, Garrett, Ed, and Hocking, Emma, 2014b, Great tsunamigenic earthquakes during the past 1,000 yr on the Alaska megathrust: Geology, v. 42, no. 8; p. 687–690. http://doi.org/10.1130/G35797.1

Shennan, Ian, Bruhn, Ronald, Barlow, Natasha, Good, Kelly, and Hocking, Emma, 2014a, Late Holocene great earthquakes in the eastern part of the Aleutian megathrust: Quaternary Science Reviews, v. 84, p. 86–97. http://doi.org/10.1016/j.quascirev.2013.11.010

Suito, Hisashi, and Freymueller, J.T., 2009, A viscoelastic and afterslip postseismic deformation model for the 1964 Alaska earthquake: Journal of Geophysical Research, v. 114, no. B11, p. 404–426, doi:10.1029/ 2008JB005954.

Suleimani, E.N., 2011, Numerical studies of tectonic and landslide-generated tsunamis caused by the 1964 Great Alaska Earthquake: Fairbanks, Alaska, University of Alaska Fairbanks, Ph.D. dissertation, 181 p.

Suleimani, E.N., Hansen, R.A., Combellick, R.A., and Carver, G.A., 2002, Tsunami hazard maps of the Kodiak area, Alaska: Alaska Division of Geological & Geophysical Surveys Report of Investigation 2002-1, 16 p., 4 sheets, scale 1:12,500. http://doi.org/10.14509/2860

Suleimani, E.N., Nicolsky, D.J., and Koehler, R.D., 2013, Tsunami inundation maps of Sitka, Alaska: Alaska Division of Geological & Geophysical Surveys Report of Investigation 2013-3, 76 p., 1 sheet, scale 1:250,000. http://doi.org/10.14509/26671

———2015, Tsunami inundation maps of Elfin Cove, Gustavus, and Hoonah, Alaska: Alaska Division of Geological & Geophysical Surveys Report of Investigation 2015-1, 79 p. http://doi.org/10.14509/29404

Suleimani, E.N., Nicolsky, D.J., Koehler, R.D., Freymueller, J.T., and Macpherson, A.E., 2016, Tsunami inundation maps for King Cove and Cold Bay communities, Alaska: Alaska Division of Geological & Geophysical Surveys Report of Investigation 2016-1, 73 p., 2 sheets, scale 1:12,500. http://doi.org/10.14509/29565

Suleimani, E.N., Nicolsky, D.J., West, D.A., Combellick, R.A., and Hansen, R.A., 2010, Tsunami inundation maps of Seward and northern Resurrection Bay, Alaska: Alaska Division of Geological & Geophysical Surveys Report of Investigation 2010-1, 47 p., 3 sheets, scale 1:12,500. http://doi.org/10.14509/21001

Synolakis, C.E., Bernard, E.N., Titov, V.V., Kânoğlu, U., and González, F.I., 2007, Standards, criteria, and procedures for NOAA evaluation of tsunami numerical models: Seattle, National Oceanic and Atmospheric Administration (NOAA)/Pacific Marine Environmental Laboratory (PMEL), Technical Memorandum OAR PMEL-135, 55 p. www.pmel.noaa.gov/pubs/PDF/syno3053/syno3053.pdf

Tang, Liujuan, Titov, V.V., Bernard, E.N., Wei, Yong, Chamberlin, C.D., Newman, J.C., Mofjeld, H.O., Arcas, Diego, Eble, M.C., Moore, Christopher, Uslu, Burak, Pells, Clint, Spillane, Michael, Wright, Lindsey, and Gica, Edison, 2012, Direct energy estimation of the 2011 Japan tsunami using deep-ocean pressure measurements: Journal of Geophysical Research, v. 117, no. C8. http://doi.org/10.1029/2011JC007635

Wang, Kelin, Wells, R.E., Mazzotti, Stephane, Hyndman, R.D., and Sagiya, Takeshi, 2003, A revised dislocation model of interseismic deformation of the Cascadia subduction zone: Journal of Geophysical Research, v. 108, no. B1, p. 2,026–2,038. http://doi.org/10.1029/2001JB001227

Watada, S., S. Kusumoto, and K. Satake, 2014, Traveltime delay and initial phase reversal of distant tsunamis coupled with the self-gravitating elastic Earth, J. Geophys. Res. Solid Earth, 119, 4287–4310, http://doi.org/10.1002/2013JB010841.

Worthington, L.L., Gulick, S.P.S., and Pavlis, T.L., 2010, Coupled stratigraphic and structural evolution of a glaciated orogenic wedge, offshore St. Elias orogen, Alaska: Tectonics, v. 29, no. 6, TC6013. http://doi.org/10.1029/2010TC002723

Worthington, L.L., Van Avendonk, H.J.A., Gulick, S.P.S., Christeson, G.L., and Pavlis, T.L., 2012, Crustal structure of the Yakutat terrane and the evolution of subduction and collision in southern Alaska: Journal of Geophysical Research, v. 117, no. B1, B01102. http://doi.org/10.1029/2011JB008493

Zweck, C., Freymueller, J.T., Cohen, S.C., 2002. Elastic dislocation modeling of the postseismic response to the 1964 Alaska earthquake, J. Geophys. Res., 2001, JB000409, 2002.

APPENDIX

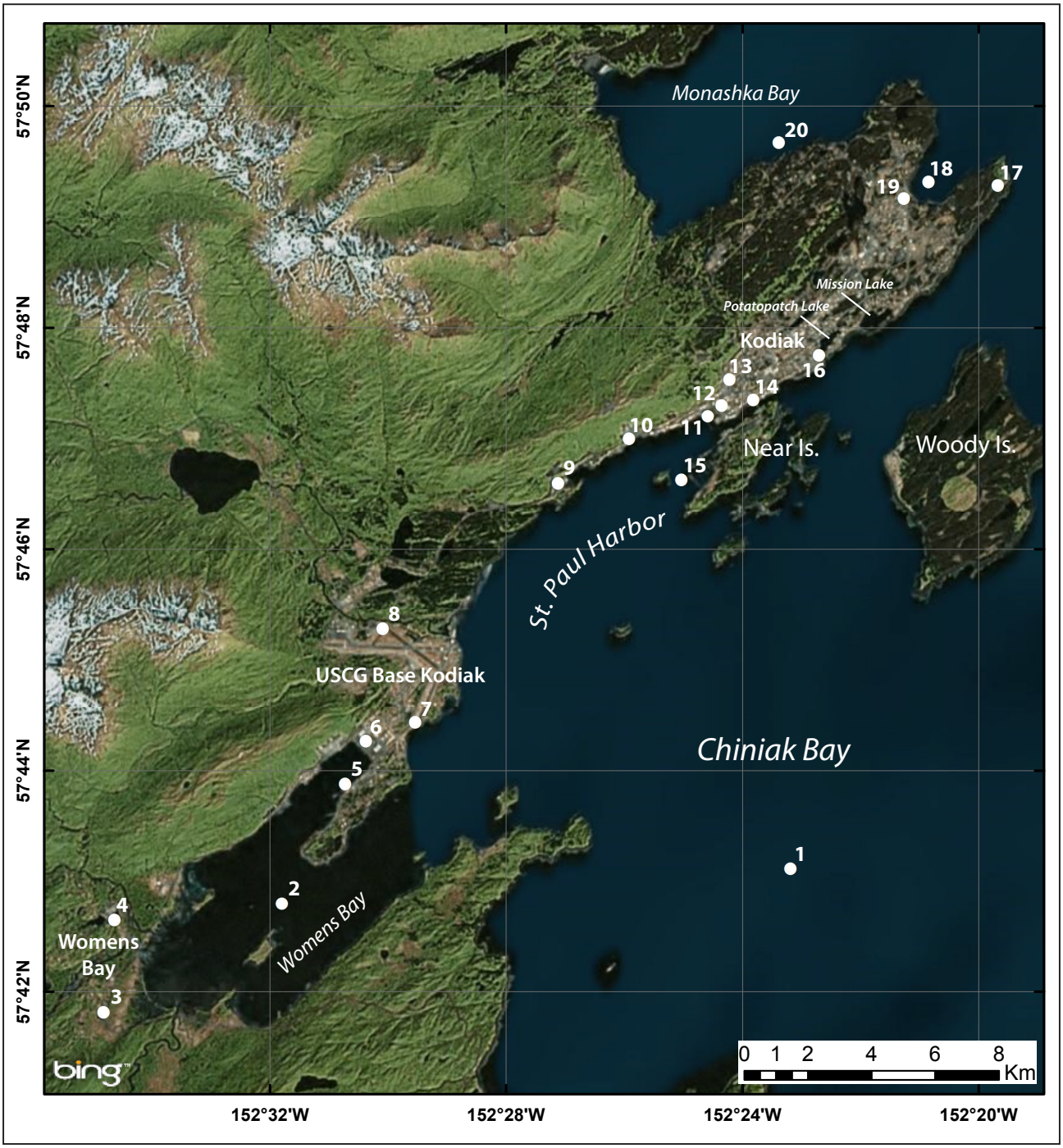

Figure A-1. Locations of time series points for Chiniak Bay and the communities of the city of Kodiak, U.S. Coast Guard Base Kodiak, and Womens Bay. The longitudinal and latitudinal coordinates of the time series points are listed in table A-1.

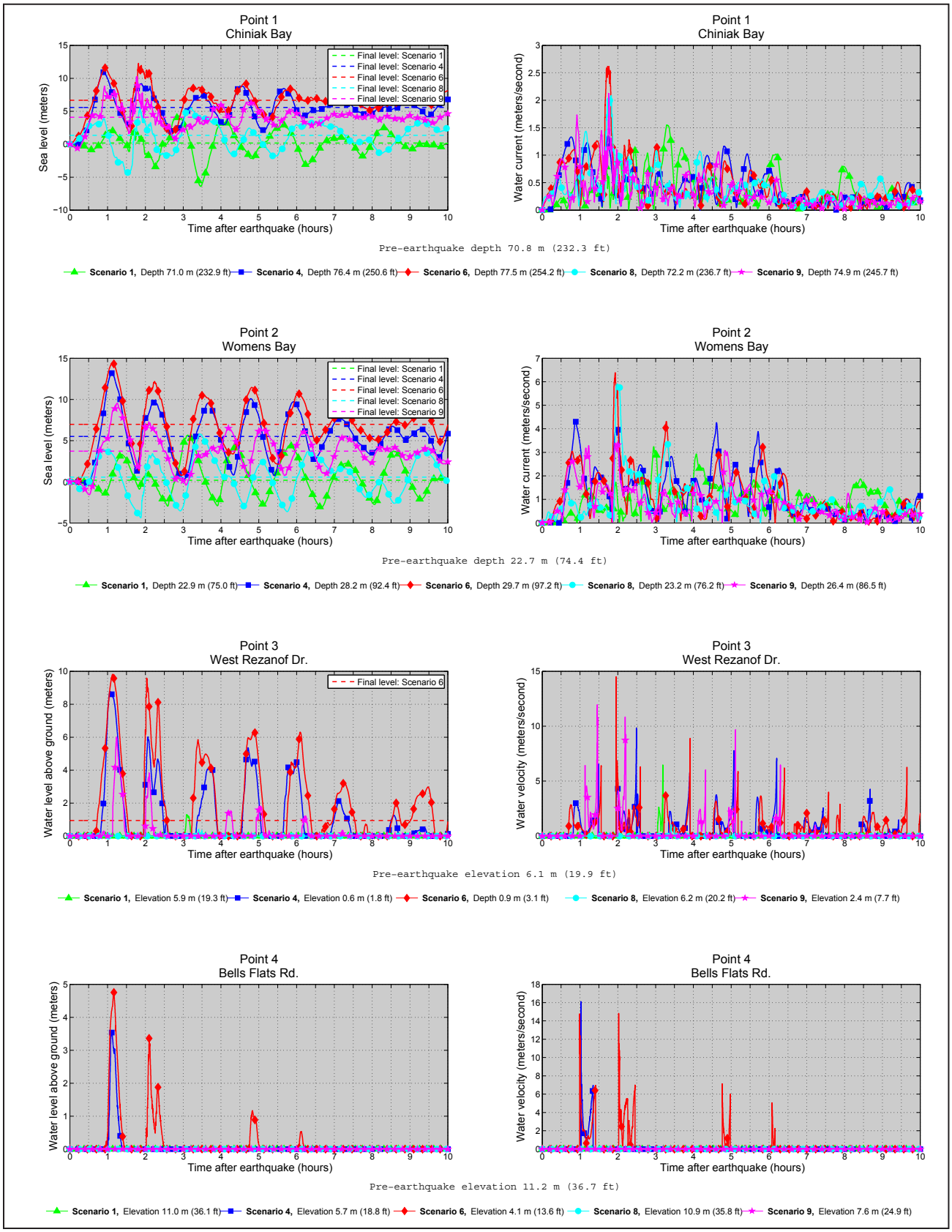

Figure A-2. Time series of water level (left) and velocity (right) for selected locations around Chiniak Bay for scenarios 1, 4, 6, 8, and 9. The pre-earthquake elevation/depth with respect to the MHHW is stated for each location. The post-earthquake elevation/depth corresponding to the MHHW datum is also listed for each scenario. For offshore locations, to show the height of an arriving tsunami, the vertical datum is such that zero corresponds to the pre-earthquake sea level. The dashed lines show the water level after the tsunami.

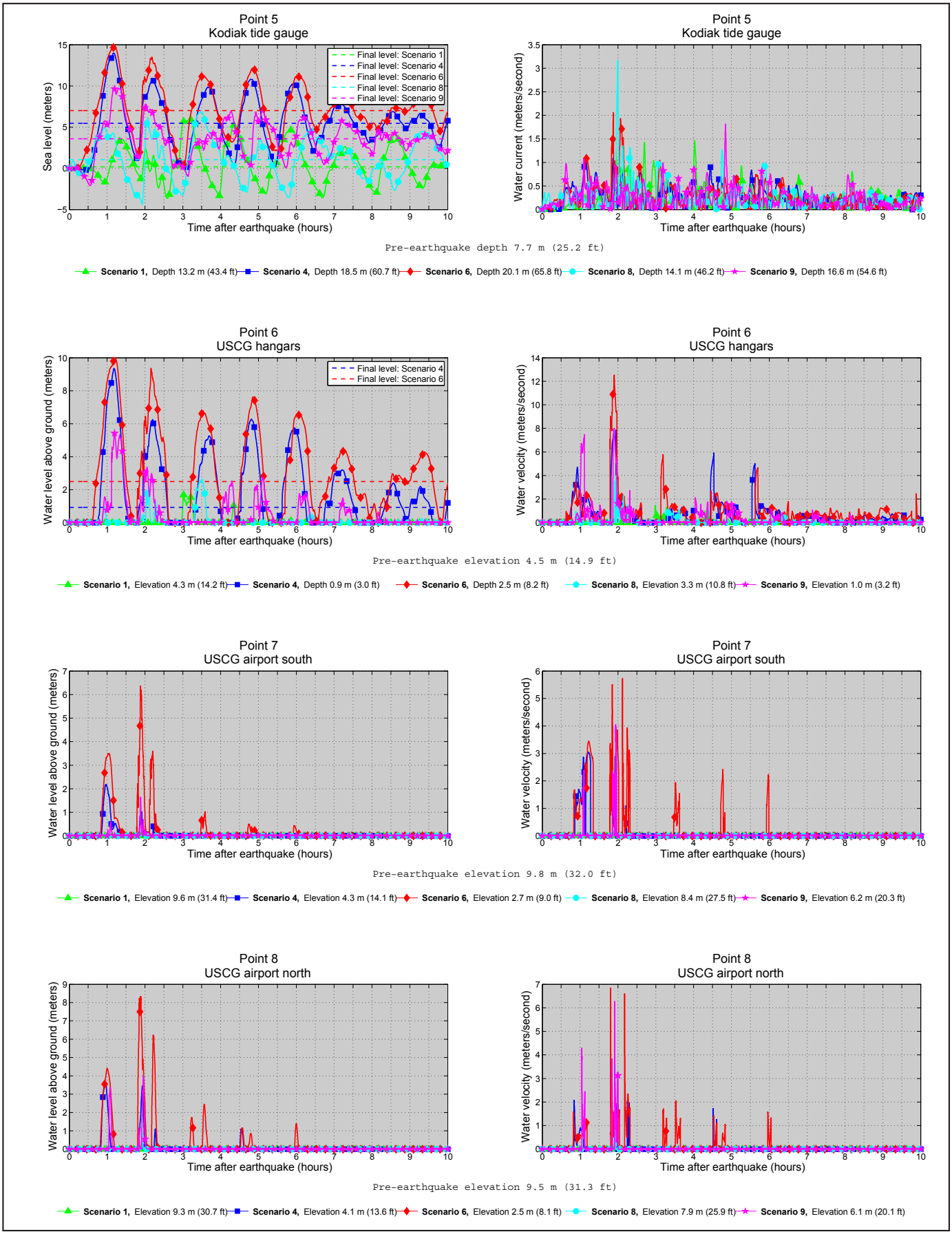

Figure A-2, continued. Time series of water level (left) and velocity (right) for selected locations around Chiniak Bay for scenarios 1, 4, 6, 8, and 9.

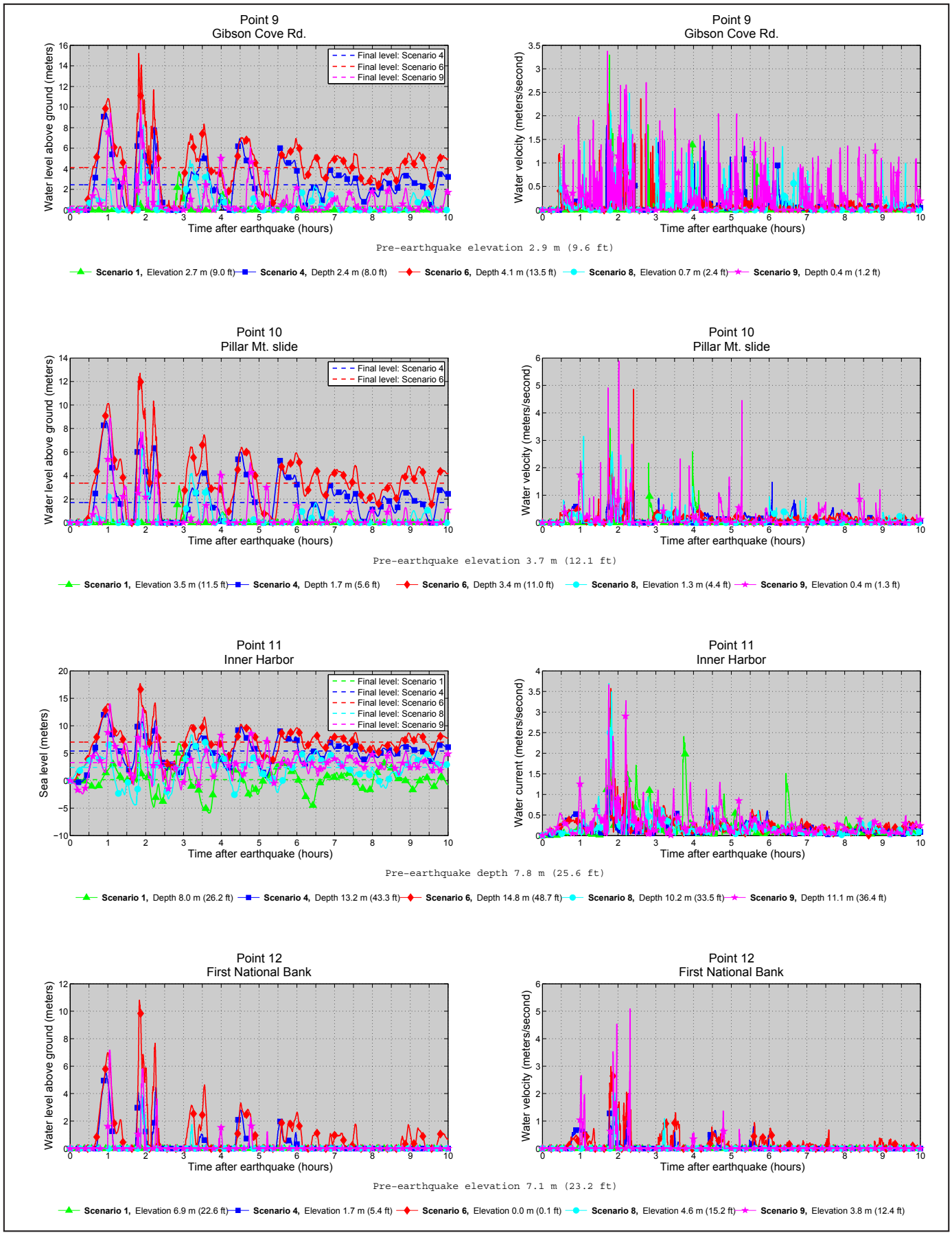

Figure A-2, continued. Time series of water level (left) and velocity (right) for selected locations around Chiniak Bay for scenarios 1, 4, 6, 8, and 9.

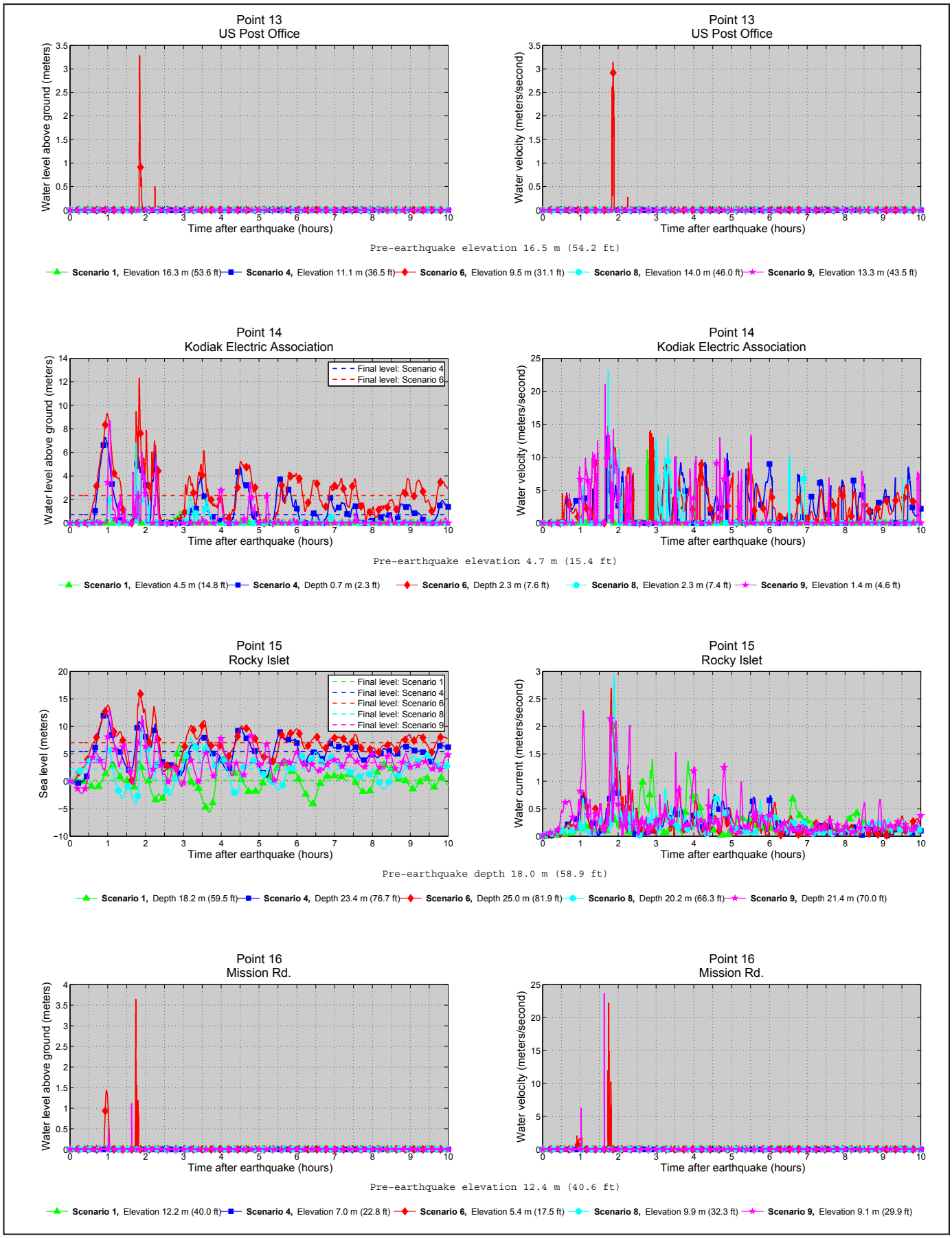

Figure A-2, continued. Time series of water level (left) and velocity (right) for selected locations around Chiniak Bay for scenarios 1, 4, 6, 8, and 9.

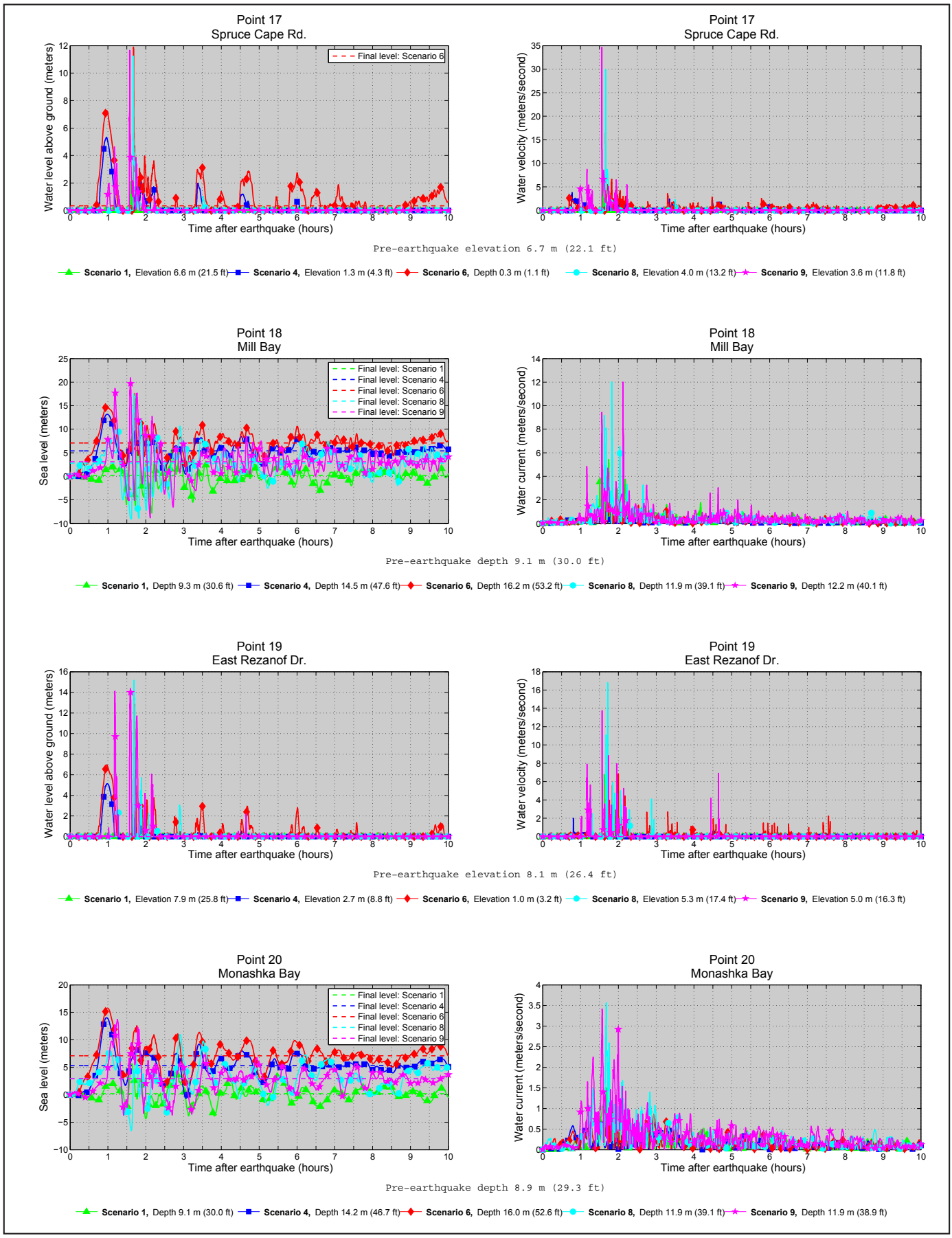

Figure A-2, continued. Time series of water level (left) and velocity (right) for selected locations around Chiniak Bay for scenarios 1, 4, 6, 8, and 9.

Table A-1. Maximum water levels at time series points around Chiniak Bay. The maximum water level above ground is provided for onshore locations, whereas the maximum water level above the pre-earthquake MHHW is provided for offshore locations. The pre-earthquake onshore (S) and offshore (O) locations are specified in the third column. The minimum elevation above the post-earthquake MHHW datum is provided for onshore locations, and the minimum post-earthquake depth is provided for offshore locations. The horizontal datum used is World Geodetic System of 1984.

#	Label	S / O	Longitude (°W)	Latitude (°N)	Minimum elevation/ depth (meters)	Maximum water depth above ground/sea level (meters)									
						Scenario									
						1	2	3	4	5	6	7	8	9	10
1	Chiniak Bay	O	152.386389	57.718611	70.8	4.4	6.3	8.8	10.9	10.4	12.3	10.6	5.5	10.2	1.3
2	Womens Bay	O	152.529722	57.713333	22.7	5.7	7.2	10.7	13.2	13.4	14.5	13.4	5.8	9.5	2.4
3	West Rezanof Drive	S	152.580000	57.696944	-0.9	1.3	3.6	7.3	8.8	9.0	9.8	8.9	0.4	6.0	0
4	Bells Flats Road	S	152.576944	57.710833	4.1	0	0	0.9	3.6	3.6	4.8	3.7	0	0	0
5	Kodiak tide gauge	O	152.511944	57.731389	7.7	6.0	8.4	11.7	14.0	13.8	14.7	14.0	6.9	9.8	2.7
6	USCG hangars	S	152.506111	57.737778	-2.5	1.7	4.0	7.1	9.3	9.2	10.0	9.4	2.6	5.5	0
7	USCG airport south	S	152.492222	57.740556	2.7	0	0.2	0.6	2.2	2.6	6.4	4.8	0	1.6	0
8	USCG airport north	S	152.501389	57.754722	2.4	0	1.5	3.0	3.7	3.7	8.3	7.1	0.9	4.0	0
9	Gibson Cove Road	S	152.451944	57.776667	-4.2	3.7	8.0	8.6	9.4	9.4	15.2	13.3	8.3	10.6	0
10	Pillar Mountain slide	S	152.431944	57.783333	-3.5	3.1	8.2	7.9	8.7	8.7	12.7	11.9	6.3	8.9	0
11	Inner Harbor	O	152.409722	57.786667	7.8	6.8	12.2	11.8	12.5	12.4	17.7	16.5	10.4	14.0	2.0
12	First National Bank	S	152.405833	57.788333	0	0	5.2	4.8	5.5	5.3	10.8	10.2	3.9	7.2	0
13	U.S. Post Office	S	152.403611	57.792222	9.4	0	0	0	0	0	3.3	3.2	0	0	0
14	Kodiak Electric Association	S	152.396944	57.789167	-2.4	1.8	5.1	6.7	7.3	7.1	12.3	10.9	6.8	8.7	0
15	Rocky Islet	O	152.417222	57.777222	18	6.6	11.1	11.5	12.4	12.2	16.6	15.5	9.4	12.9	2.0
16	Mission Road	S	152.378333	57.795833	5.3	0	0	0	0	0	3.6	1.6	0	1.1	0
17	Spruce Cape Road	S	152.328056	57.821389	-0.4	2.1	3.1	3.0	5.3	6.3	11.9	9.3	11.2	11.6	0
18	Mill Bay	O	152.347500	57.821944	9.1	8.3	12.1	11.7	13.2	14.7	17.6	16.0	17.5	20.9	1.8
19	East Rezanof Drive	S	152.354444	57.819444	0.9	2.1	5.5	3.8	5.1	6.7	12.9	11.2	15.2	14.4	0
20	Monashka Bay	O	152.389722	57.827778	8.9	5.6	11.3	12.2	14.0	15.4	15.8	17.0	10.9	13.7	1.5

Table A-2. The maximum water velocity at time series points around Chiniak Bay. The pre-earthquake onshore (S) and offshore (O) locations are specified in the third column. The minimum elevation above the post-earthquake MHHW datum is provided for onshore locations, and the minimum post-earthquake depth is provided for offshore locations. The horizontal datum used is World Geodetic System of 1984.

#	Label	S / O	Longitude (°W)	Latitude (°N)	Minimum elevation/ depth (meters)	Maximum water velocity (meters/second)									
						Scenario									
						1	2	3	4	5	6	7	8	9	10
1	Chiniak Bay	O	152.386389	57.718611	70.8	1.5	2.3	1.7	1.4	1.2	2.6	2.5	2.1	2.1	0.3
2	Womens Bay	O	152.529722	57.713333	22.7	3.2	3.9	4.5	4.3	4.6	6.4	5.3	5.9	3.4	1.2
3	West Rezanof Drive	S	152.580000	57.696944	-0.9	6.5	10.3	12.0	9.8	9.7	14.5	12.8	1.0	11.9	0
4	Bells Flats Road	S	152.576944	57.710833	4.1	0	0	13.4	16.1	14.3	14.8	14.6	0	0	0
5	Kodiak tide gauge	O	152.511944	57.731389	7.7	1.5	2.8	1.7	1.1	0.9	2.1	1.8	3.2	1.8	0.4
6	USCG hangars	S	152.506111	57.737778	-2.5	1.5	6.4	7.9	7.9	8.1	12.5	10.9	4.0	8.0	0
7	USCG airport south	S	152.492222	57.740556	2.7	0	0	2.7	3.0	3.1	5.7	5.7	0	4.0	0
8	USCG airport north	S	152.501389	57.754722	2.4	0	2.6	2.6	2.1	1.9	6.8	7.3	3.6	6.3	0
9	Gibson Cove Road	S	152.451944	57.776667	-4.2	3.3	3.3	2.0	1.8	1.2	2.4	4.2	2.5	3.4	0
10	Pillar Mountain slide	S	152.431944	57.783333	-3.5	3.4	7.4	3.5	1.5	0.8	4.9	4.2	3.1	5.9	0
11	Inner Harbor	O	152.409722	57.786667	7.8	2.8	5.3	2.0	1.1	0.9	3.6	3.5	3.7	3.7	0.6
12	First National Bank	S	152.405833	57.788333	0	0	2.2	1.7	1.5	1.2	3.0	3.1	2.0	5.1	0
13	U.S. Post Office	S	152.403611	57.792222	9.4	0	0	0	0	0	3.1	3.2	0	0	0
14	Kodiak Electric Association	S	152.396944	57.789167	-2.4	13.4	16.3	17.2	13.2	12.8	14.7	19.0	23.1	21.1	0
15	Rocky Islet	O	152.417222	57.777222	18.0	1.4	2.8	2.5	1.1	0.8	2.7	3.6	2.9	2.3	0.4
16	Mission Road	S	152.378333	57.795833	5.3	0	0	0	0	0	22.2	12.3	0	23.6	0
17	Spruce Cape Road	S	152.328056	57.821389	-0.4	8.2	6.3	4.1	3.8	4.4	16.5	20.5	29.9	34.6	0
18	Mill Bay	O	152.347500	57.821944	9.1	5.4	6.5	1.7	1.0	0.5	4.0	3.6	12.0	12.0	0.4
19	East Rezanof Drive	S	152.354444	57.819444	0.9	6.8	9.7	6.1	4.2	2.0	6.9	7.3	16.8	13.7	0
20	Monashka Bay	O	152.389722	57.827778	8.9	1.5	1.8	0.9	0.7	0.5	1.1	1.1	3.6	3.4	0.3